International Journal of
Molecular Sciences

MDPI

Article

Isolation and Characterization of Antibodies Against Vascular Cell Adhesion Molecule-1 Reveals Putative Role for Ig-like Domains 2 and 3 in Cell-to-Cell Interaction

Binura Perera [1,2,3], Yuao Wu [2,3], Jessica R. Pickett [2,3], Nadya Panagides [1], Francisca M. Barretto [4], Christian Fercher [1,4], David P. Sester [5], Martina L. Jones [1,4], Hang T. Ta [2,3] and Lucia F. Zacchi [1,4,6,*]

1 ARC Training Centre for Biopharmaceutical Innovation, Australian Institute for Bioengineering and Nanotechnology, The University of Queensland, St. Lucia, QLD 4072, Australia; binura.perera@griffithuni.edu.au (B.P.); n.panagides@outlook.com (N.P.); c.fercher@uq.edu.au (C.F.); martina.jones@uq.edu.au (M.L.J.)
2 Queensland Micro- and Nanotechnology Centre, Griffith University, Nathan, QLD 4111, Australia; yuao.wu@griffith.edu.au (Y.W.); jessica.pickett@griffithuni.edu.au (J.R.P.); h.ta@griffith.edu.au (H.T.T.)
3 School of Environment and Science, Griffith University, Nathan, QLD 4111, Australia
4 Australian Institute for Bioengineering and Nanotechnology, The University of Queensland, St. Lucia, QLD 4072, Australia; f.barretto@student.uq.edu.au
5 Flow Cytometry Suite, Translational Research Institute, Woolloongabba, QLD 4102, Australia; dpsester@gmail.com
6 School of Chemistry and Molecular Biosciences, The University of Queensland, St. Lucia, QLD 4072, Australia
* Correspondence: l.zacchi@uq.edu.au; Tel.: +61-7-334-63149

Abstract: The vascular cell adhesion molecule-1 (VCAM-1) plays an important role in inflammation, where it facilitates the recruitment of leukocytes to the inflamed area via leukocytes' VLA-4 and endothelial cells' VCAM-1 interaction. VCAM-1 expression is also upregulated in certain cancers. VCAM-1 has seven Ig-like domains, with domains 1 and 4 shown to be critical for VLA-4 binding. However, the specific functions of individual VCAM-1 Ig-like domains remain poorly understood. In this study, we identified single-chain variable fragment (scFv) antibodies targeting domains 2, 3, and 5 of VCAM-1, and investigated the ability of these antibodies to block VCAM-1-mediated cell adhesion to macrophages. We show that scFv antibodies against Ig-like domains 2 and 3 interfere with the ability of macrophages to bind endothelial cells, suggesting that these domains also play a role in facilitating this interaction. These results emphasize the need to more carefully study the role of each domain on VCAM-1 function and highlight the potential of targeting these VCAM-1 domains for more tailored therapeutic interventions in inflammatory diseases and cancer.

Keywords: VCAM-1; scFv; Ig-like domains; macrophage attachment

Citation: Perera, B.; Wu, Y.; Pickett, J.R.; Panagides, N.; Barretto, F.M.; Fercher, C.; Sester, D.P.; Jones, M.L.; Ta, H.T.; Zacchi, L.F. Isolation and Characterization of Antibodies Against Vascular Cell Adhesion Molecule-1 Reveals Putative Role for Ig-like Domains 2 and 3 in Cell-to-Cell Interaction. *Int. J. Mol. Sci.* **2024**, *25*, 13650. https://doi.org/10.3390/ijms252413650

Academic Editor: Albrecht Reichle

Received: 29 November 2024
Accepted: 13 December 2024
Published: 20 December 2024

1. Introduction

Vascular cell adhesion protein 1 (VCAM-1) is a cell adhesion molecule implicated in a range of diseases, including atherosclerosis, immunological disorders (e.g., rheumatoid arthritis (RA) and asthma), and cancer, among others [1–3]. VCAM-1 is expressed in a variety of cells and tissues, including endothelial cells. VCAM-1 expression is induced by proinflammatory cytokines [3] and it is involved in the recruitment of leukocytes during inflammation [2]. For example, during atherosclerosis, endothelial cells express VCAM-1, and this assists in the migration of monocytes to the atherosclerotic plaque [1]. Therefore, VCAM-1 expression can be correlated with the extent of plaque formation, making VCAM-1 an ideal biomarker for atherosclerosis [1,3,4]. VCAM-1 expression is also upregulated on the endothelium of rejected transplanted organs [3], and in breast cancer [5], lung cancer [6], and colorectal cancer [7]. Due to its role in a range of physiological and medical conditions, VCAM-1 has received considerable attention in the last decades.

VCAM-1 is a 90 kDa type I transmembrane glycoprotein and a member of the immunoglobulin (Ig) superfamily of proteins [8]. VCAM-1 interacts with cell surface proteins such as integrin $\alpha_1\beta_4$ (VLA-4), one of the main binding partners, as well as other integrin and non-integrin proteins such as Galectin-3 (in eosinophils), and SPARC/osteonectin, among others [1–3,9–12]. VCAM-1 interacting proteins are critical during inflammation, as they promote leukocyte migration/transvasation [12–16]. VCAM-1 interaction with (some) protein ligands leads to downstream signaling resulting in cytoskeleton re-organization and loosening of cell-to-cell junctions, which facilitates leukocyte transvasation [17]. VCAM-1 is composed of 3–7 Ig-like domains, a single transmembrane domain, and a 19 amino acids cytoplasmic domain [1,8,18]. Human VCAM-1 is expressed as either seven (7D) or six (6D) Ig-like domain containing forms, while mouse VCAM-1 has a 7D and a truncated 3D form [8,18,19]. In humans, the full-length 7D form, rather than the 6D form, is predominantly expressed [8,20]. The 7D protein shows efficient binding to VLA-4 and is the primary mediator of cell adhesion [9,21]. The 6D VCAM-1 does not contain domain 4, and shows less efficient cell adhesion, with decreasing efficiency of binding under increasing shear force [1,21]. VCAM-1 can be proteolytically cleaved near the transmembrane domain by matrix metalloproteinases (MMPs), including the sheddase ADAM17 [22,23], resulting in a soluble VCAM-1 version [24]. The level of soluble VCAM-1 6D form increases in certain pathologies such as RA and systemic lupus erythematosus [25,26]). There is high sequence similarity between Ig-like domains 1 and 4, 2 and 5, and 3 and 6, due to a proposed intragene duplication event [18]. Of all duplicated domain pairs, domains 1 and 4 share the highest sequence similarity [27], and these domains are also involved in the interaction of VCAM-1 with VLA-4, expressed in leukocytes [8,9,28]. Domain 2 appears to be structurally required for domain 1 function, and specific residues in domain 2 are involved in the interaction with VLA-4 ($\alpha_1\beta_4$) and, more importantly, with $\alpha_4\beta_7$ [29,30]. The interaction with Galectin-3, on the other hand, typically requires LacNAc disaccharides (Galβ1-4GlcNAc) found internally in *N*- or *O*-linked glycans [14], suggesting that human VCAM-1 could bind Galectin-3 through its Ig-like domains 3, 4, 5, and/or 6, which carry 1, 1, 2, and 2 *N*-linked glycans, respectively. On the other hand, domain 6 of VCAM-1 appears to be a key target for TNFα-induced angiogenesis [31], and the antibody blockade of domain 6 impairs leukocyte transmigration but not adhesion, as well as lung cancer cell migration [3,6,32]. To date, the functional roles of only some of the VCAM-1 domains have been elucidated.

Due to the important role of VCAM-1 in a range of pathologies, several antibodies targeting VCAM-1 have been developed [1] (see Supplementary Table S1). Anti-VCAM-1 antibodies have been tested in mouse models for their effectiveness against asthma [33] and atherosclerosis [34,35]. Further, there are promising in vitro studies that utilize radiolabeled anti-VCAM-1 antibodies to target and treat early-stage brain metastases [36]. In addition, diagnostic ELISA kits for VCAM-1 expression have been used in multiple clinical trials (clinicaltrials.gov). Clearly, VCAM-1 antibodies play important roles both in the laboratory and the clinic.

Identifying new antibodies against membrane targets can be challenging. Monoclonal antibodies (mAbs) are typically derived from single B cell/hybridoma clones [37,38] or from phage display libraries [39]. One key aspect required for any successful antibody discovery campaign is antigen presentation. The antigen should ideally be presented to the polyclonal antibody pools as close to its native conformation as possible, which can be difficult in the case of membrane proteins due to their hydrophobic transmembrane domain(s) [40]. To ensure native conformation, membrane proteins can be expressed on the surface of cells or other membrane environments such as nanodiscs [41]. Phage display biopanning is an excellent in vitro platform for the discovery of new antibodies against both soluble and membrane-bound targets like VCAM-1, and several mAbs derived from phage display biopanning have been approved for clinical use [42,43].

Discovering antibodies against VCAM-1 is important not only due to the potential medical applications of targeting VCAM-1, but also to understand the biological function of

this important molecule. Since the late 1980s, several groups have published anti-VCAM-1 antibodies (see Supplementary Table S1). These antibodies bind VCAM-1 domains 1, 4, and 6, or within the 1–3 and 4–7 domains of the molecule (Supplementary Table S1), and have shed light on the functional aspects of VCAM-1. However, specific functional contributions of some VCAM-1 Ig-like domains (such as domains 3, 5, and 7) and their association with cell binding and intracellular signal transduction remain understudied. To increase the toolbox of antibodies that recognize the specific Ig-like domains of VCAM-1, we performed phage display biopanning using a naïve human phage display library [40] and panned against membrane-bound mouse 7D VCAM-1. We identified multiple scFv antibodies that bind Ig-like domains 2, 3, or 5. We show here that scFv antibodies binding Ig-like domains 2 and 3 significantly reduce the in vitro binding of macrophages to activated endothelial cells. These results suggest that mVCAM-1 Ig-like domains 2 and 3 play important functional roles, that these antibodies could help obtain a clearer picture of the structure–function relationship between VCAM-1 Ig-like domains and VCAM-1 physiological roles, and that antibodies targeting these domains could have diagnostic and/or therapeutic potential.

2. Results

2.1. Identification of Binders to mVCAM-1 Through Phage Display Biopanning

To identify scFv binders to mouse 7D VCAM-1 (mVCAM-1), we used a human naïve phage display library [44] and we panned against full-length mVCAM-1 transiently expressed in mammalian cell lines. Whole-cell phage display biopanning allows the expression of VCAM-1, a transmembrane glycoprotein with multiple disulphide bonds, in its native conformation with adequate post-translational modifications [40]. The full open reading frame (ORF) of the 7 Ig-like domain mVCAM-1 was fused with a C-terminal eGFP protein to monitor transfection efficiency, observe mVCAM-1 subcellular localization, and for effective cell sorting through FACS. Importantly, the VCAM-1 C-terminus is intracellular, and we expected no impact of the independently folding eGFP protein on VCAM-1 biosynthesis and trafficking. Indeed, VCAM-1-eGFP expressed and trafficked to its expected plasma membrane localization with efficiency (Figure 1D–F and Supplementary Figure S1). We performed whole cell biopanning using the Jones–Mahler human naïve scFv library (JM library) [44], and alternating mammalian cell lines (CHO XL99 cells for round 1 and HEK293 suspension cells for round 2). Alternating cell lines during cell-based biopanning facilitates the depletion of irrelevant cell surface binders due to the differences in the surface proteome among the different cell lines, thereby improving enrichment of relevant binders [40]. To check for enrichment of phages against mVCAM-1 in our phage pools and select a phage pool for screening, we performed polyclonal flow cytometry on the original library and the sub-libraries (Figure 1). We looked for an increase in the % of GFP+/Phage+ events (top right quadrant of the graphs, Figure 1) in transfected cells, indicating phage binding to cells with high mVCAM-1-eGFP expression (Figure 1D–F). The JM library did not show specific phage binding to mVCAM-1 (Figure 1D, 1.75% of events in GFP+/Phage+ quadrant) or non-transfected cells (Figure 1A, 0.04% of events in Phage+ quadrant), as expected. The round 1 and 2 phage pools showed increased unspecific cell surface-binding to untransfected cells, also as expected since phage-binding cell surface mammalian proteins will also be enriched in this method (Figure 1B,C, 15.3% and 22% events in GFP-/Phage+ quadrant, respectively). However, we observed a clear increase in mVCAM-1 phage-binding in Round 2 phage pool compared to the JM library and Round 1 phage pools (Figure 1D–F, 1.75% vs. 3.29% and 27.9% events in GFP+/Phage+ quadrant, respectively), with some background binding observed, as expected (Figure 1D–F, 0.9%, 5.73%, and 10.1% events in GFP-/Phage+ quadrant). This result indicated that the biopanning campaign was successful, and that we had effectively enriched for anti-VCAM-1 binding phages after two rounds of panning. To note, generally, three or four rounds of biopanning are required for enrichment of scFv-phages against a target; however, we obtained a clear enrichment of the library on Round 2, a result likely associated with the quality and size of the antigen and its presentation format (Figure 1D–F). Performing further

rounds of biopanning could have led to the isolation of phages with higher affinity/avidity for mVCAM-1, but this also risked reducing sequence variability in isolated phages and our chances of isolating binders to different regions of mVCAM-1 (a key goal of this work).

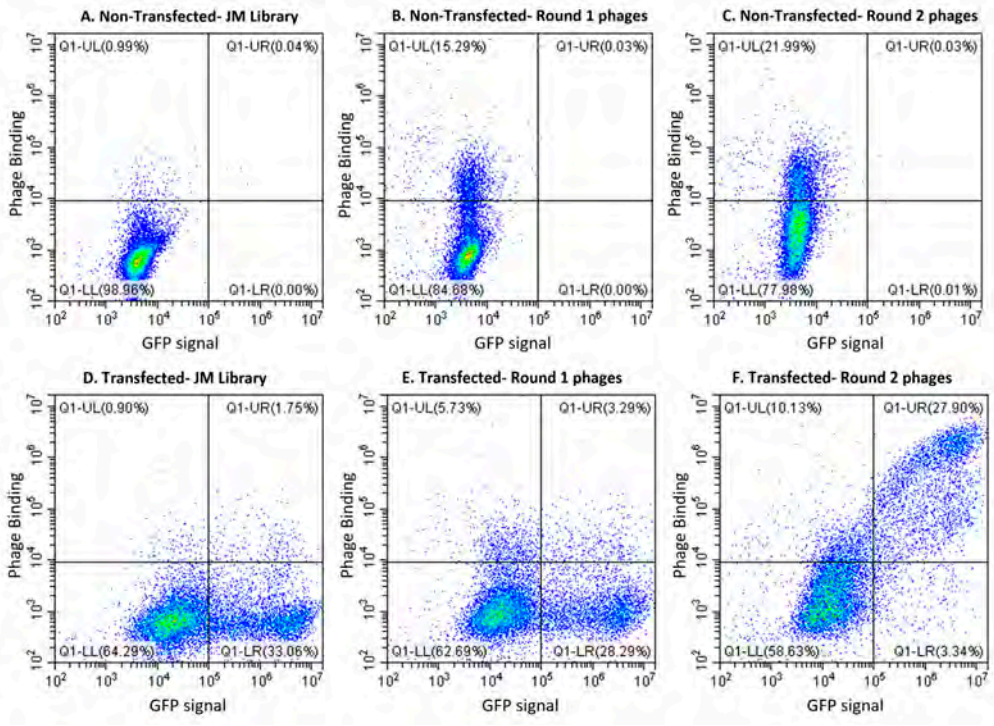

Figure 1. Flow cytometry analysis of the phage pools showed enrichment of anti-VCAM-1 phages in the round 2 phage pool. CHO XL99 cells non-transfected (**A**–**C**) or transfected with pEGFP-N1-mVCAM-1 (**D**–**F**) were incubated with the Jones–Mahler human naïve phage library (JM library) (**A**,**D**), round 1 phage pool (**B**,**E**), or round 2 phage pool (**C**,**F**). The plots depict GFP expression (x-axis) vs. phage binding (y-axis).

To identify specific mVCAM-1 phage binders, we first screened a total of 262 phage clones from the round 2 phage pool by monoclonal whole cell ELISA and identified several positive clones (~6% positive clones) (Supplementary Figure S2). Next, we sequenced the scFv encoding DNA of the positive clones to identify unique clones. Multiple sequence alignment of the translated amino acid sequences of the clones identified eight unique scFv sequences (Supplementary Figure S2, identified with numbers). The sequences for clones 1A9 and 2E6 were identified multiple times, while the other six sequences were represented only once. The coding regions of the scFvs were confirmed by IgBlast (IgBlast tool (nih.gov). Clones 1A9 and 2B9 had a kappa light chain, while the other six clones had a lambda light chain. Clones 2D3 and 3H4 shared the highest total sequence similarity among all eight clones (Supplementary Figure S3, left), with identical complementary determining regions (CDR) 1 and 2 in the heavy chain as well as high total sequence similarity in their light chains (Supplementary Figure S3, right). Clones 2E2 and 2E6 shared an almost identical lambda light chain (Supplementary Figure S3, right). Clones 2D8 and 1A9 had identical CDR2 in the heavy chain, but all other CDR sequences differ. All eight clones had a unique CDR3 in the heavy chain (Supplementary Figure S3, middle), which is one of the most critical determinants of antibody specificity [45]. Together, these results suggest that each individual scFv likely binds to different mVCAM-1 epitopes and/or with varying affinities.

We used flow cytometry to confirm that all positive phage clones bound to mVCAM-1-eGFP transiently expressed on the surface of CHO XL99 cells (Figure 2, red). Some background binding to non-transfected cells was observed for some clones (2D8, 2E2, and 3H4), possibly due to the "sticky" nature of the phages and slight differences in sample processing (Figure 2, blue). We observed two different binding patterns for the phages

(Figure 2), as follows: while most phages followed a linear relationship between the phage signal and GFP signal that eventually saturated and plateaued, some phages such as 2E2 and 2D3 showed a biphasic curve in which higher mVCAM-1-eGFP expression was required to observe phage binding (Figure 2D,F). This result may suggest differences in binding strength for mVCAM-1 by the different phage clones (possibly due to differences in affinity of the scFvs for VCAM-1 or differences in the number of scFvs displayed on the phage surface), or differences in epitope availability. In summary, we performed two rounds of whole cell biopanning using a human naïve phage display library and mammalian cells transiently expressing mVCAM-1, and isolated eight unique scFv sequences that bind the 7D mVCAM-1 isoform.

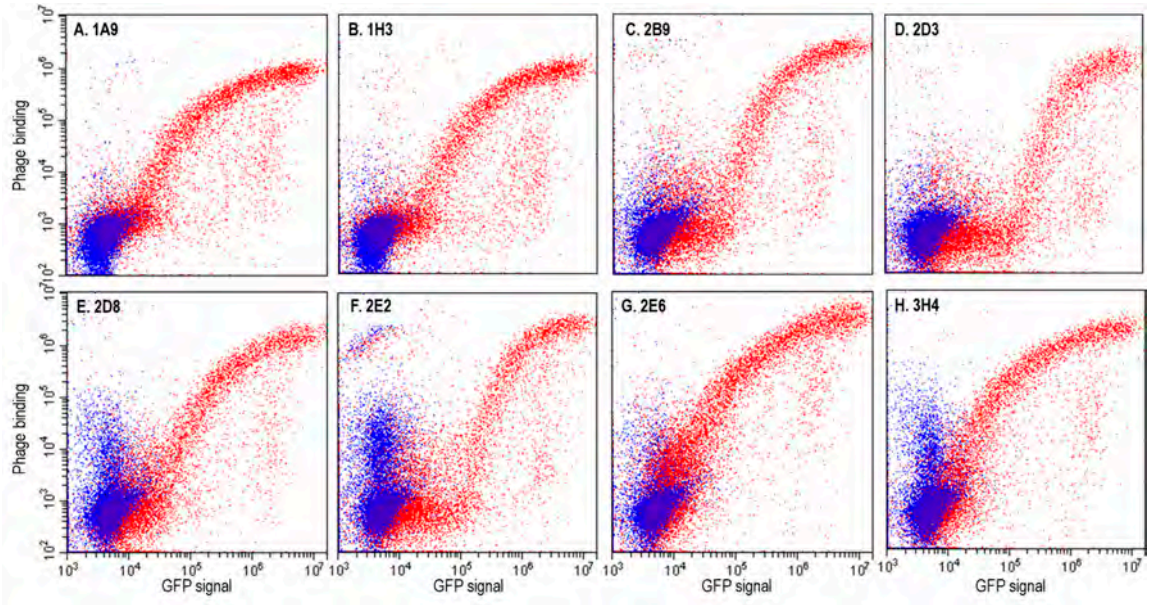

Figure 2. Monoclonal flow cytometry confirmed the positive phage clones bound to mVCAM-1. Positive phage clones from round 2 phage pool selected by whole-cell ELISA were tested for binding to mVCAM-1 by flow cytometry using CHO XL99 cells transfected with mVCAM-1-eGFP (red) or not (blue). Shown are the 8 unique clones selected (**A**) 1A9, (**B**) 1H3, (**C**) 2B9, (**D**) 2D3, (**E**) 2D8, (**F**) 2E2, (**G**) 2E6, and (**H**) and 3H4. The plots depict GFP expression (x-axis) vs. phage binding (y-axis).

During DNA sequence analysis, we also noticed that the amino acid sequence of clones 1H3 and 2B9 contained undesired sequence liabilities. Clone 1H3 had two Cys residues located within its CDR3-H which could lead to alterations in antibody-binding specificity due to non-native disulfide bond formation and/or folding defects. On the other hand, clone 2B9 had an *N*-linked glycosylation sequon in CDR2-H which could be occupied following expression in eukaryotic cells. The presence of an *N*-linked glycan could impact folding, expression, and/or binding of 2B9 antibodies to the target. Therefore, the 1H3 and 2B9 clones were not further pursued.

2.2. Verifying Expression and mVCAM-1 Binding for All Unique scFv-LPETGs

The other six unique clones were subcloned into a pET28b(+)-LPETG vector. The LPETG tag is a sequence of five amino acids that can be used for sortase-mediated antibody conjugation [46,47], allowing the construction of, for example, antibody drug conjugates and other chimeras. The tag is located exactly between the end of the scFv sequence and the LEHHHHHH C-terminal end containing the 6xHis tag, with no additional sequences, and its presence did not impact expression compared to non-LPETG tagged scFvs. These scFv-LPETG antibodies were expressed in *E. coli* SHuffle, a strain that promotes the formation of disulphide bonds in the cytoplasm, which are essential for scFv antibodies. The size of the scFv-LPETGs was calculated by ProtParam to be ~ 27 kDa (Supplementary Table S4), as

expected for scFvs. Expression of the scFv-LPETGs in *E. coli* SHuffle cells was followed by protein extraction and purification using a HisTrap column, dialysis, and concentration (Supplementary Figure S4). All scFv-LPETGs were successfully expressed and purified from bacteria.

To verify that the purified scFv-LPETG antibodies bound mVCAM-1 when not associated with a phage particle, we again performed flow cytometry (Figure 3). Non-transfected cells (negative control), and cells transfected with mVCAM-1-eGFP were incubated with purified scFv-LPETGs, and then stained with mouse anti-His antibody followed by anti-mouse IgG-Dylight650 antibody. As expected, all unique scFv-LPETGs showed binding to mVCAM-1, with only minor background binding of some of the antibodies to untransfected cells (Figure 3). The linear vs. biphasic cell-binding patterns previously observed for the phages were still observed with the purified scFv-LPTEG antibodies, indicating that this is a property of the scFv and not of the phage-bound scFv clones (Figures 2D,F and 3B,D, clones 2D3 and 2E2). In conclusion, all selected scFvs were expressed in bacteria and bound mVCAM-1 expressed in CHO cells in the native membrane environment.

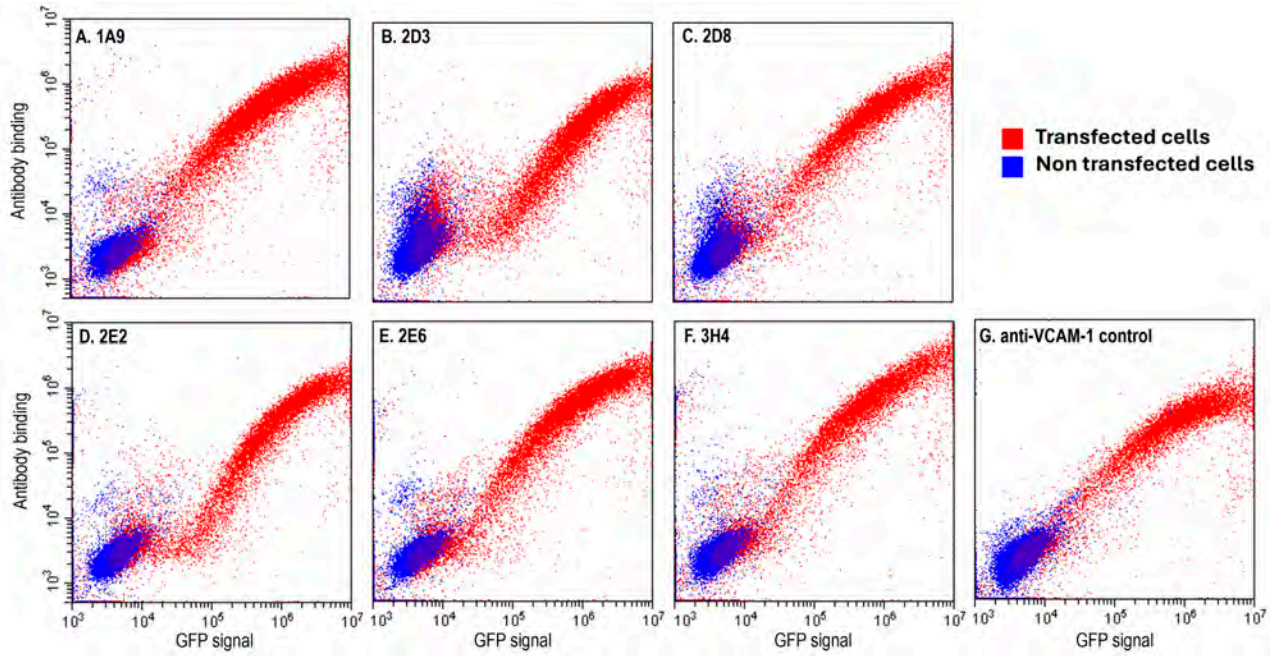

Figure 3. Purified scFv-LPETGs bind mVCAM-1. ExpiCHO cells transiently transfected with mVCAM-1-eGFP (red) or not (blue) were stained with purified scFv-LPETGs. The scFvs were detected with a mouse anti-HIS antibody and goat anti-mouse Dylight650. Shown are the 6 unique clones (**A**) 1A9, (**B**) 2D3, (**C**) 2D8, (**D**) 2E2, (**E**) 2E6, and (**F**) 3H4, and (**G**) anti-VCAM-1 CBL1300 as positive control. The plots depict GFP expression (x-axis) vs. antibody binding (y-axis).

2.3. Ig-like Domain Antibody Binding Mapping

VCAM-1 has seven Ig-like domains, some of which have been associated with different functions (Supplementary Table S1). To determine to which mVCAM-1 Ig-like domain the discovered antibodies bind, we generated a suite of mVCAM-1 mutants in which up to four different Ig-like domains were simultaneously deleted from mVCAM-1 (as depicted in Figure 4A). Although all constructs were eGFP tagged, it was possible that some of the mutations led to lower cell surface expression while not substantially reducing intracellular GFP signal (Supplementary Figure S5). To ensure that all the deletion mutants were expressed on the cell surface, we inserted an N-terminal FLAG tag between the signal sequence and the first Ig-like domain in all constructs and performed flow cytometry using an anti-FLAG antibody (Figure 4A,B). Addition of the FLAG-tag did not appear to negatively influence the cell surface expression levels of the wild-type (WT) construct (compare

anti-VCAM-1 binding to the untagged and FLAG-tagged WT constructs, Figure 4A,B, Supplementary Figure S6). As expected, the anti-FLAG antibody bound to all constructs (Figure 4B, Supplementary Figure S6), demonstrating that all constructs were expressed on the cell surface. However, the Δ5–7, Δ6–7, and Δ7 constructs showed weaker anti-FLAG binding when compared to the WT construct, with the Δ5–7 construct being the most impacted (Figure 4B, Supplementary Figure S6), indicating lower cell surface expression of these mutants. This result was not due to lower overall construct expression, since the GFP signal in the cells transfected with the mutants was similar or higher than in the WT controls (Supplementary Figure S5). Further, since the Δ5 construct showed similar or higher anti-FLAG binding than the Δ6–7 and Δ7 constructs (Figure 4B, Supplementary Figure S6), it was not the deletion of domain 5 that led to the substantially lower expression levels in the Δ5–7 mutant (Figure 4B). While the lower expression of the Δ5–7 mutant could impact the ability of the antibodies to recognize the remaining Ig-like domains on this construct, the availability of the other well-expressed constructs was enough to provide certainty regarding the location of the (main) antibody-binding site in the mVCAM-1 molecule.

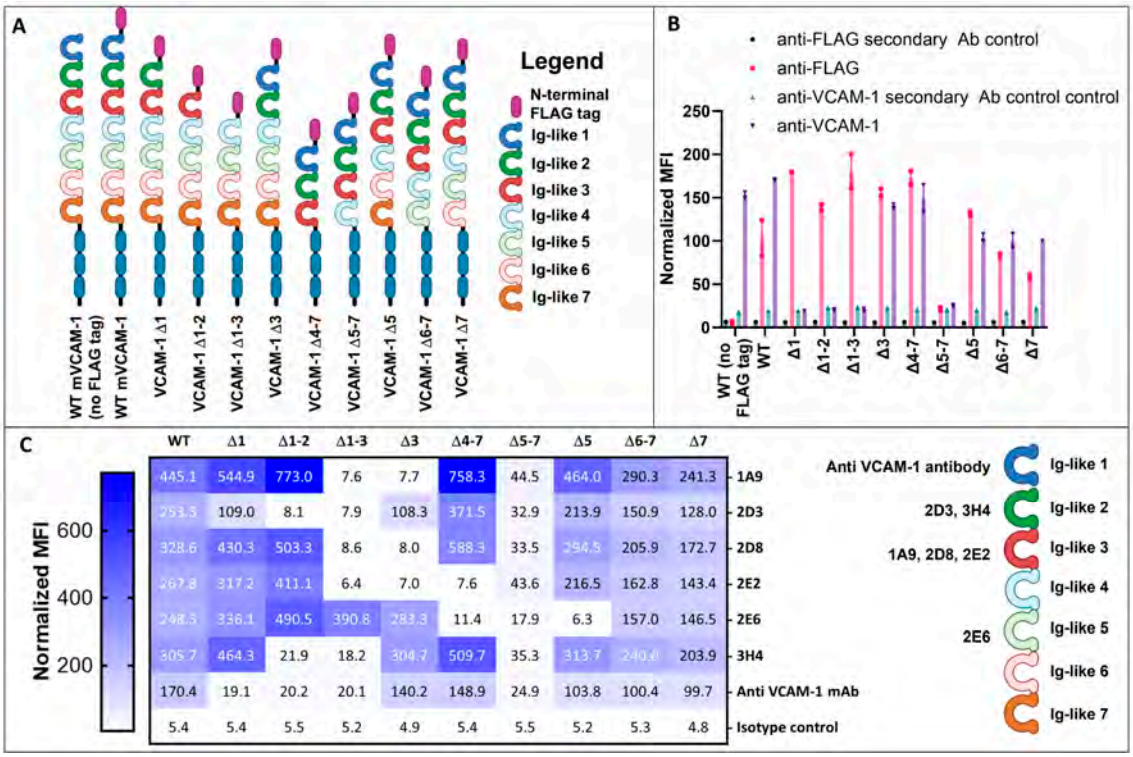

Figure 4. Ig-like domain mapping of the isolated antibodies. (**A**) Schematics of mVCAM-1 Ig-like domain deletion mutants used in this study. (**B**,**C**) Flow cytometry analysis of the binding of the commercial anti-mVCAM-1 antibody (CBL1300) (**B**,**C**), anti-FLAG (**B**), and our new full-length IgG2a reformatted antibodies (**C**) to cells transiently transfected with mVCAM-1-eGFP WT (with or without N-terminal FLAG) or FLAG-tagged Ig-like deletion constructs. Overall, VCAM-1 cell surface expression was determined using anti-FLAG antibody or anti-VCAM-1 CBL1300 antibody (**B**). CBL1300 required a different secondary antibody control than the FLAG antibody; therefore, results with its own secondary antibody-only control are also shown (**B**). (**C**) Table showing the normalized MFI values for each of the VCAM-1/antibody combinations (also see Supplementary Figure S8). The color scheme correlates with MFI value, with lighter colors indicating lower antibody binding and darker colors indicating higher antibody binding. On the right, a schematic representation of the mVCAM1 Ig-like domain structure shows the (tentative) binding location for the different antibodies tested in this study. Displayed is the average normalized MFI-Max-Min (mVCAM-1-eGFP-positive, antibody-positive cells normalized to MFI of the mVCAM-1-eGFP-negative, antibody-negative cells) from one experiment with 2 replicates. Schematics were created with BioRender.com.

Flow cytometry analysis of the CBL1300 (M/K2) rat anti-VCAM-1 antibody showed strong binding to the WT and the Δ4–7, Δ6–7, and Δ7 constructs (Figure 4C, Supplementary Figure S6). Binding of this antibody to the Δ5–7 construct was poor, similar to what was observed with the anti-FLAG antibody (Figure 4B,C, Supplementary Figure S6). The commercial antibody did not bind the Δ1, Δ1–2, and Δ1–3 constructs, showing similar binding as the secondary antibody-only control for those mutants (Figure 4B, Supplementary Figure S6). These results indicate that the anti-VCAM-1 commercial antibody binds to the Ig-like domain 1 in mVCAM-1, as previously shown (Supplementary Table S1), validating our experimental design.

For this flow cytometry experiment, we used the full-length mouse IgG2a reformatted versions of the scFvs (Supplementary Figure S7). As we hoped, the results demonstrate that the antibodies bound to different Ig-like domains (Figure 4C, Supplementary Figure S8). Antibodies 1A9, 2D8, and 2E2 appeared to bind the Ig-like 3 domain of mVCAM-1 (Figure 4C, Supplementary Figure S8), since they were able to bind to all constructs except for the Δ1–3, Δ2–3 and Δ3 constructs (Figure 4C, Supplementary Figure S8). Interestingly, antibody 2E2 also showed reduced binding to the Δ4–7 construct, suggesting that the binding site may include Ig-like domain 4, or may be affected by its deletion due to a conformational/structural change or to altered availability due to enhanced proximity to the cell membrane of the Δ4–7 construct (Figure 4C, Supplementary Figure S8). On the other hand, antibodies 2D3 and 3H4 appeared to bind the Ig-like domain 2, since they were able to bind all constructs except for the Δ1–2 and Δ1–3 constructs (Figure 4C, Supplementary Figure S8). To note, however, 2D3 also showed somewhat lower binding relative to the WT construct for the Δ1 mutant, suggesting that the binding site for 2D3 may be close to and/or involve a portion of the Ig-like 1 domain or connecting region, or alternatively that the absence of domain 1 impacts the binding site of 2D3 (Figure 4C, Supplementary Figure S8). Interestingly, as discussed above, sequence alignment of 3H4 and 2D3 showed that they share an almost identical heavy chain variable region (except for CDR3-H), and the highest similarity in light chains among all analyzed scFvs (Supplementary Figure S3), which could explain the similar, but not identical, binding to mVCAM-1. Finally, the 2E6 antibody appeared to bind the Ig-like 5 domain, since it was able to bind all constructs except for the Δ4–7, Δ5–7, and Δ5 constructs (Figure 4C, Supplementary Figure S8). Similar to the results with the anti-FLAG and commercial anti-VCAM-1 antibodies, none of our antibodies was able to bind well to the Δ5–7 mutant (Figure 4C, Supplementary Figure S8), probably due to the poor cell surface expression and potential associated folding issues in this construct (see above). We note that it is possible that some or all of the antibodies tested here are also able to bind (albeit less strongly) to their corresponding duplicated, yet not identical, Ig-like domain (i.e., 2 and 5, and 3 and 6 [18]). However, potential binding to the duplicated Ig-like domain was not observed in this experiment, either because of low sequence similarity at the specific epitopes or due to the signal being below the limit of detection for this assay. In conclusion, we were able to isolate multiple antibodies that bind to different Ig-like domains of mVCAM-1, including Ig-like domains 2, 3, and 5 (Figure 4C, Supplementary Figure S8).

2.4. scFv Antibodies Against VCAM-1 Ig-like Domains 2 or 3 Can Block Macrophage Attachment to Endothelial Cells

Blocking different Ig-like domains in VCAM-1 with antibodies can lead to different functional impacts, depending on where the antibody binds, and this has been clearly shown for Ig-like domains 1, 4, and 6 [1,8,9,28,32] (Supplementary Table S1). One of the most important physiological roles of VCAM-1 is to facilitate macrophage recruitment into an inflammatory site [1]. Here, we tested if the antibodies we identified had an impact on the binding of macrophages to activated endothelial cells natively expressing 7D mVCAM-1. We performed this analysis using the scFv-LPETGs instead of the full-length antibodies to reduce the possibility of steric hindrance of the full-length antibody on mVCAM-1/ligand interactions, and thereby increase the certainty of a direct impact of Ig-like domain blocking

on the attachment phenotype. To do this, SVEC4-10 endothelial cells were treated with LPS for 24 h to induce mVCAM-1 cell surface expression [48]. Next, different scFv-LPETGs were supplemented to the medium and cells were incubated for 2 h to block mVCAM-1. Then, the DiOC6-labelled macrophages were cocultured with endothelial cells for 10 min. Green fluorescence on the cell culture layer after washes represents macrophages that remained attached to the endothelial cells. As expected for a full-length antibody-binding VCAM-1 Ig-like 1 domain (Figure 4, Supplementary Table S1), treatment with the commercial anti-mVCAM-1 significantly reduced the macrophage ability to attach to endothelial cells compared to the non-antibody control, as demonstrated by a significant reduction in green fluorescence intensity (Figure 5, $p < 10^{-4}$). Also as expected, the non-anti-VCAM-1 scFv antibody control did not significantly alter macrophage attachment, and its MFI value was similar to the non-antibody control (Figure 5). Interestingly, all anti-VCAM-1 scFv-LPETGs reduced macrophage attachment to endothelial cells and, with the exception of 2E6 ($p = 0.056$), the other 5 scFv-LPETG antibodies significantly reduced macrophage attachment when compared to the non-antibody-treated control (Figure 5). Together, the results show that scFv antibodies able to bind domains other than 1, 4, and 6 [1,8,9,28,32] can also reduce macrophage attachment to endothelial cells in vitro.

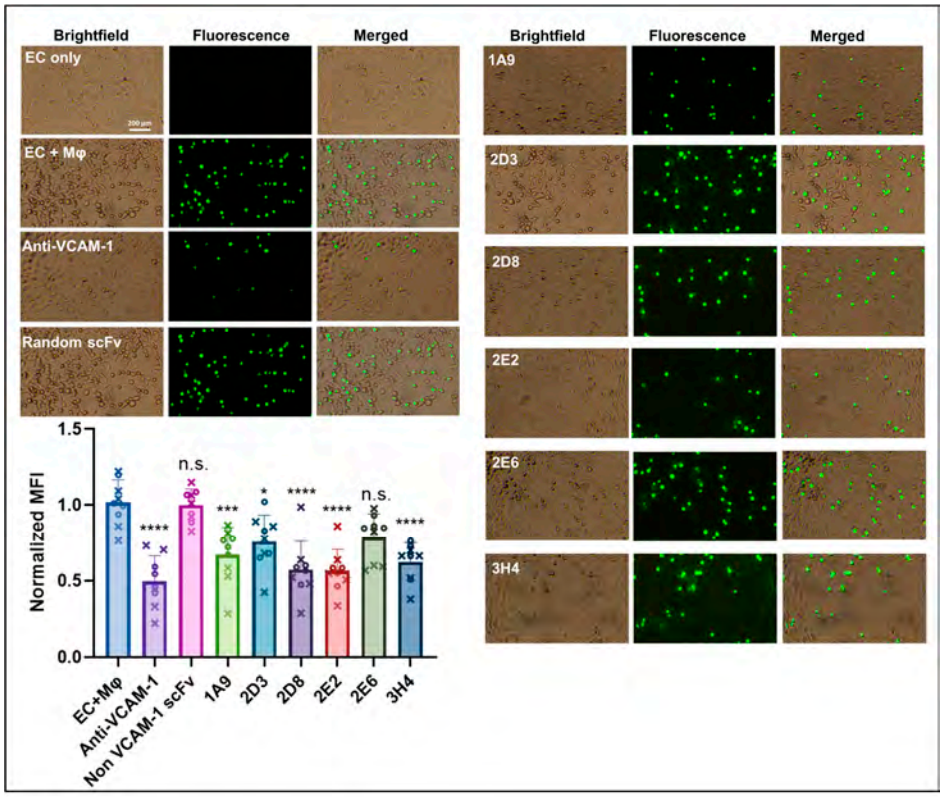

Figure 5. Anti-VCAM-1 scFvs targeting Ig-like domains 2 or 3 significantly decrease macrophage attachment to endothelial cells. Representative images from brightfield and green fluorescence, as well as their merged counterparts, show the attachability of macrophage J774A.1 cells (green) to activated SVEC4-10 endothelial cells (EC) after treatment with our different antibodies and control antibodies (20 μg/mL). A non-antibody treatment and a random (non-VCAM-1 binder) scFv treatment were used as negative controls, while treatment with commercial full-length anti-mVCAM-1 (CBL1300) was used as positive control. Displayed is the average normalized MFI +/− SEM of two experiments with 4 (each data point shown with a circle) or 5 (each data point shown with an x) replicates each, n = 9. The data were normalized by dividing each individual replicate to the mean of the non scFv-treated control (EC + Macrophage) within each repeat. All statistical comparisons are to the EC + macrophage control (one-way ANOVA followed by post-hoc Tukey pairwise comparisons): * $p < 0.05$, *** $p < 0.001$, **** $p < 0.0001$; n.s. not significant.

3. Discussion

In this project, we sought to identify antibodies that can bind mVCAM-1 at different Ig-like domains, which could be used to better dissect the biological function of different parts of VCAM-1 or for clinical applications. VCAM-1 is a cell surface glycoprotein implicated in the adhesion of white blood cells to endothelial cells during inflammatory processes. Due to VCAM-1's role in a myriad of diseases, this molecule has been extensively studied and it has been targeted for therapeutic and diagnostic applications [1]. Multiple antibodies against VCAM-1 have been raised since this molecule was identified in the late 1980s ([49], Supplementary Table S1), and these have been in part used to study VCAM-1's function. In some cases, both the binding site of these antibodies to VCAM-1 domains (especially to domains 1, 4, and 6) and the functional consequences of antibody binding are known, allowing a clear link between structure and function of VCAM-1 (Supplementary Table S1) [1,8,9,19,27–29,32–34,48–60]. However, in many other cases, only either the functional impact of antibody binding or the potential antibody binding site on VCAM-1 has been described, or neither information is available (Supplementary Table S1) [26,58,61–63]. In fact, the biochemical and biological role of most VCAM-1 domains remains poorly defined. In this study, we developed a suite of antibodies that bind to Ig-like domains 2, 3, or 5 of mouse VCAM-1 (with no apparent cross-reactivity with other VCAM-1 domains), which we hope will aid to more clearly dissect VCAM-1 molecular interactions, signal transduction, and physiological roles, and which may be used for downstream clinical applications.

The most highly expressed version of VCAM-1 in cells contains 7 Ig-like domains [8,18,19]. The function of Ig-like domains 1 and 4 has been thoroughly characterized, as they contain the binding site for one of VCAM-1's most important binding partners, VLA-4 [1,8,9,28]. Domain 2 appears to also be important for binding of $\alpha_1\beta_4$ and, mainly, $\alpha_4\beta_7$ integrins [29,30]. In addition, VCAM-1 also mediates endothelial cell-eosinophil interaction [56,60,64], potentially through an interaction between eosinophils' Galectin-3 [11,13,14] and VCAM-1's Ig-like domains 3, 4, 5, and 6, which harbor sites for *N*-linked glycosylation. Interestingly, given *N*-linked glycosylation's innate environment-dependent macro and microheterogeneity [65], the multiple potential sites for glycosylation in VCAM-1 could be powerful drivers of functional diversity in VCAM-1/Galectin-3 interactions. Domain 6, on the other hand, appears to be associated with TNFα-induced angiogenesis [31], and it is important for leukocyte transvasation but not adhesion [32]. Pepinsky et al. [50] identified two protease-sensitive sites in 7D VCAM-1, one site between Ig-like domains 3 and 4 and one within two highly conserved cysteines in domain 5 (arguing for an unusual lack of disulfide bond formation in that Ig-like domain in VCAM-1). The functional implications of the biochemical characteristics of these two VCAM-1 regions are still unclear, but indicate differences in folding and accessibility to other proteins, including potential extracellular proteases that may regulate extracellular VCAM-1 shedding [50], internalization/degradation, and/or protein-protein interactions in a redox-sensitive manner. In addition, here we observed that deletion of domains 5, 6, and 7 together led to a reduction in cell surface expression of VCAM-1 (Figure 4B, Supplementary Figure S6). Even more, while the anti-VCAM-1 CBL1300 antibody bound well the Δ5, Δ7 and Δ6–7 mutants, this antibody bound the Δ5–7 mutant less efficiently (Figure 4B, Supplementary Figure S6), suggesting inappropriate folding of VCAM-1 or inaccessibility of the antibody to domain 1, which is the main binding site of CBL1300 (Figure 4B, Supplementary Figure S6, and Supplementary Table S1). A similar phenotype was observed with our 6 antibodies (Figure 4C and Supplementary Figure S8). We note that a secreted C-terminally Fc-tagged VCAM-1 construct carrying a Δ5–7 Ig-like domain deletion can be purified [32,34]; however it is possible that the Fc C-terminal tag aided in this construct's solubility and expression as a secreted molecule, which is different from our membrane bound construct. In fact, our results support Pepinsky et al. conclusion that VCAM-1 conformation depends on its C-terminal portion [50], and suggest a complex relationship among the last three Ig-like domains in determining expression and/or conformation of the full-length VCAM-1 molecule. Altogether, our results and

those of others argue for the need for a more detailed exploration of the biological roles of all VCAM-1 domains.

To identify new antibodies against VCAM-1 we performed phage display biopanning using a human naïve library, which is an animal-free platform for the discovery of monoclonal antibodies [40–42,44,66–68]. Biopanning is an affinity screening process which allows for the in vitro isolation of antibody-expressing phages from a phage display library that are specific to a target of interest [42,68]. The target antigen was full-length mouse 7D VCAM-1, a type-I transmembrane glycoprotein, and was presented through expression on the surface of mammalian cell lines, thereby ensuring its correct folding and post-translational modifications. Two rounds of biopanning were enough to generate an enriched pool of scFv-phages against mVCAM-1 (Figure 1). A third round of biopanning would have allowed us to further enrich the phage sub-library for anti-mVCAM-1 binders, but this may have also led to a reduction in the diversity of the scFv-phage population by selecting against weaker or more poorly expressed binders that may bind different parts of mVCAM-1. We identified several antibodies that bound mVCAM-1 as scFv-phage (Figure 2), as scFv (Figure 3), and as full-length mAb (Figure 4). Two of the scFv-phage binders were not pursued, due to the presence of sequences in their CDRs that could lead to potential folding/binding errors (clones 1H3 and 2B9) when expressed in bacteria and/or mammalian cells. Three of the 6 antibodies identified bound mVCAM-1 Ig-like 3 domain: 1A9, 2D8, and 2E2; two bound Ig-like 2 domain: 2D3 and 3H4; and one bound Ig-like 5 domain: 2E6 (Figure 4). Interestingly, all antibodies reduced macrophage attachment to endothelial cells when compared to the non-antibody-treated control (EC + macrophage), with five of them significantly reducing macrophage attachment: clones 1A9, 2D3, 2D8, 2E2, and 3H4, which are Ig-like domain 2 or 3 binders (Figure 5, $p < 0.05$, Supplementary Figure S8; we note that clone 2E6 (an Ig-like 5 domain binder) showed $p = 0.056$). Similar results were obtained when the full-length IgG2a versions of these antibodies were tested in the same assay, except that all full length-antibodies, including clone 2E6, significantly reduced macrophage attachment to endothelial cells (Pickett et al., manuscript in preparation). Different VCAM-1-binding antibodies will require different concentrations to exert a functional effect due to different affinities for the antigen (a property of the paratope/epitope sequence and of accessibility to the epitope). An antibody titration experiment would allow for a more detailed comparison of the different antibodies. Overall, our results show that blocking other Ig-like domains beyond 1 and 4 [1,9,21,28] can also reduce cell-to-cell attachment (Figures 4 and 5).

There are multiple ways in which anti-VCAM-1 antibodies could impact VCAM-1-mediated attachment and transmigration. Hession et al. [19] hypothesized early on that VCAM-1 may play other roles beyond being an adhesin, including participating on signal transduction. Indeed, VCAM-1 activation leads to cytoskeleton remodeling and changes at the endothelial cell junctions [69,70], and antibodies against VCAM-1 can affect VCAM-1 downstream signaling [17,34,70]. Some of the ways antibodies can alter VCAM-1 function is by directly or indirectly blocking protein–protein interactions or by altering VCAM-1 downstream signaling in a ligand-independent manner. To do this, antibodies could block access to residues involved in the interaction, or alter VCAM-1 epitope accessibility, folding/conformation, quaternary structure (homo or hetero multimerization), or cell surface expression by, e.g., triggering VCAM-1 internalization. For example, our Ig-like 2 domain binders could be blocking attachment by preventing proper interaction with $\alpha_4\beta_7$ integrin [30]. Additional experiments using molecular docking, mutagenesis, and structural biology to dissect antibody–VCAM-1 interactions, a more detailed study of the precise VCAM-1 epitope to which each antibody is binding, and the functional impact of changes on/blocking of these domains on protein–protein interactions, cellular physiology, and downstream signaling will help in understanding the structure–function relationship of each VCAM-1 Ig-like domain and how antibodies impact them. Given that scFvs are considerably smaller than full-length monoclonal antibodies (~25 kDa vs. ~150 kDa, respectively), the chances that the impact of a monomeric scFv on attachment is due to the

steric hindrance of the VLA-4/VCAM-1 interaction is low (although this would have to be demonstrated biochemically, which lies outside the scope of this manuscript). Thus, the antibodies described in this work could help uncover new VCAM-1 biology (binding partners and/or function).

Gaining a deeper knowledge of VCAM-1 functions would not only facilitate our general understanding of physiology and biology, but it would also provide key information for the design of precision therapies targeting specific structural domains associated with specific clinical outcomes. Competition studies with purified VLA-4 or other known binders and antibodies would help elucidate potential novel mechanisms of action. In addition, researchers could harness the power of omic techniques and AI to perform a more comprehensive spatial and temporal interactomic, transcriptomic, proteomic, phosphoproteomic, and/or glycoproteomic profiling of VCAM-1 (WT and Ig-like domain mutants) and downstream signaling pathways, in the presence or not of ligands and/or anti-VCAM-1 antibodies. These analyses could help uncover signaling pathways, new interacting proteins, and the function of specific Ig-like domains. Analyses targeting post-translational modifications in VCAM-1 or its ligands are especially important for understanding how these modifications impact VCAM-1 function in health and disease (e.g., during cancer or inflammation). These antibodies could also help better dissect the role of VCAM-1 amino acid sequences involved in ligand interaction [30]. Despite the large amount of data already acquired on VCAM-1, there is still plenty to learn about this molecule's physiological roles.

Antibodies against VCAM-1 could have a range of clinical applications in cardiovascular disease, cancer, and inflammatory diseases. For instance, it would be interesting to test these antibodies in preclinical animal models of atherosclerosis. The antibodies (either in IgG or scFv formats) can also be used as antibody–drug conjugates, to specifically deliver payloads with anti-cancer or anti-inflammatory properties. However, further studies need to be conducted to determine whether binders also exert an activating function, since downstream signaling may be counterproductive to the desired clinical outcome. Anti-VCAM-1 antibodies could also be used for diagnostic purposes, to identify VCAM-1 expressing cancer or atherosclerotic plaques, etc. Cross-reactivity of these antibodies with other Ig-like domain containing proteins could be a potential issue that may require further in silico and in vitro testing before moving into pre-clinical models. Further progression into clinical studies would require the identification of cross-reacting antibodies to both mouse and human VCAM-1. Anti-VCAM-1 antibodies could have a range of therapeutic, diagnostic, or theranostic applications.

For the purpose of the functional assays, this work focused on scFv anti-VCAM-1 versions, rather than the full-length antibodies, for two main reasons. First, if an impact on attachment was observed with the scFv, this impact would also be highly likely to be observed with the full-length antibody, while the reverse is not necessarily true. Second, scFvs have many advantages over full-length antibodies in terms of biochemistry and pharmacokinetics [71,72]. A typical mammalian IgG antibody is a large molecule consisting of two heavy chains linked to each other and to a light chain by disulphide bonds [38,71–73]. On the other hand, an scFv is a small functional antigen binding domain that consists of one variable heavy and one variable light domain joined by a peptide linker, ~1/6th the size of a full length IgG [71,72,74]. Compared to full-length antibodies, the smaller size of scFvs allows for better tissue penetration and rapid clearance while maintaining target binding specificity [71,72,75]. The enhanced tissue penetration is especially advantageous in some pathologies such as cancer [76] and atherosclerosis [35], in which scFvs can reach the tumor or plaque core better than full-length antibodies [71,72,75,77]. Further, rapid clearance is useful when antibodies are carrying a toxic payload (e.g., for radioactive immunotherapy or diagnostics) [78]. The scFvs also have reduced immunogenicity and no effector function, since they lack the Fc region [79]. There are many differences between scFv and full-length antibodies, and the decision on which kind of antibody to use will ultimately depend on the specific biochemical test required or desired therapeutic modality.

Here, we showed that scFvs targeting different Ig-like domains of VCAM-1 that are not directly associated with the VLA-4/VCAM-1 interaction can also negatively impact macrophage-endothelial cell attachment (Figures 4 and 5). Our data emphasize that there is still plenty to learn about VCAM-1 biological function, and our antibodies are excellent tools to facilitate future studies. Given the critical role this molecule plays in a myriad of physiological and disease states, understanding its biochemical characteristics and molecular interactions will be key to designing more precise and targeted future therapies.

4. Methodology

4.1. Plasmid Construction and Site-Directed Mutagenesis

All vectors used in this study are described in Supplementary Table S2 and mutagenesis primers are described in Supplementary Table S3. The pUCIDT-Amp vector containing the *Mus musculus* VCAM-1 open reading frame (UniProt accession ID P29533) codon optimized for expression in Chinese Hamster Ovary (CHO) cells was purchased from Integrated DNA Technologies (IDT) (see Supplementary Materials for full mVCAM-1 sequence). mVCAM1 was subcloned from pUCIDT-Amp-VCAM-1 (LZCBI17) into pEGFP-N1 through NheI and BamHI double restriction digestion and ligation to generate full-length mVCAM1 C-terminally tagged with eGFP (LZCBI18).

mVCAM-1 Ig-like domain deletion mutants (LZCBI121-127 and LZCBI129-130) were constructed by deletion of 1 or more of the 7 Ig-like domains, similar to a previously published strategy [32]. The description of the mutagenesis strategy can be found in the Supplementary Materials.

Phagemids from selected phage clones were extracted using Qiagen QIAprep Spin Miniprep kit (Qiagen, Germantown, MD, USA, 27104) following the manufacturer's protocol and sequenced as previously described [40,41]. The DNA encoding the selected scFvs was subcloned from the phagemid vectors into pET28b(+)-LPETG vector (a modified Novagen vector that incorporates a C-terminal LPETG tag, as described in the Supplementary Information) through NcoI and NotI double restriction digestion and ligation. The scFv sequences obtained were reformatted into full-length mouse IgG2a monoclonal antibodies (Supplementary Table S2) using the InFusion HD cloning kit (Takara Bio USA, Inc., San Jose, CA, USA, 639648), following previously published methodologies [41,80].

All clones made in this study were sequenced to ensure the correct DNA sequence.

4.2. Mammalian Cell Culture Maintenance and Transfection

Chinese hamster ovary (CHO) XL99 and human endothelial kidney (HEK) 293 cell lines were maintained in CD CHO medium (Gibco™, Waltham, MA, USA, 10743029) or FreeStyle™ 293 Expression medium (Gibco™, 12338018), and supplemented with 0.4% (*v*/*v*) anti-clumping agent (Gibco™, 0010057DG) and GlutaMAX™ Supplement (Gibco™, 35050061). ExpiCHO cells were maintained on ExpiCHO medium as described by the manufacturer (Thermo Fisher, Waltham, MA, USA, A29131). Cells were routinely grown at 37 °C, 7.5% CO_2, and 125 rpm. Adherent CHO-K1 cells were maintained in Ham's F-12K (Kaighn's) Medium (Gibco™, 21127022) supplemented with 10% Fetal Bovine Serum (FBS) (Gibco™, 10099141) and incubated at 37 °C, 7.5% CO_2.

CHO XL99 and HEK293 cells were transfected using a DNA/polyethyleneimine (PEI)-Max complex, as previously described [41]. For transfection of CHO-K1 cells, 1.4×10^6 CHO-K1 adherent cells were seeded into T25 flasks and incubated overnight at 37 °C, 7.5% CO_2. The next day, pEGFP-N1-mVCAM-1 or pEGFP-N1 (negative control) plasmids were transfected into CHO-K1 cells using Lipofectamine™ 3000 Reagent (Invitrogen™, Waltham, MA, USA, L3000001) and OptiMEM™ Reduced Serum Medium (Gibco™, 31985062) and following the manufacturer's procedure. ExpiCHO cells were transfected as per the manufacturer's instructions using an ExpiFectamine CHO Transfection kit (Thermo Fisher, A29131). Expression of VCAM-1_eGFP and mutants was monitored using BioRad ZOE™ Fluorescent Cell Imager (Bio-Rad, Hercules, CA, USA) and by flow cytometry (see below).

Macrophage J774A.1 cells and SVEC4-10 endothelial cells (CRL-2181) were obtained from the American Type Culture Collection. The J774A.1 cells were maintained in a non-treated 100 × 20 mm cell culture dish (Corning®, Corning, NY, USA, 430591) containing RPMI 1640 (Thermo Fisher, LTS11875093) with 10% fetal calf serum (Thermo Fisher, 10099141), penicillin (100 U/mL) (Thermo Fisher, 15140122), and 1% L-glutamine (Thermo Fisher, 25030081), and cultured in an incubator at 37 °C, 5% CO_2. The SVEC4-10 cells were maintained in tissue culture-treated T75 flask (Sarstedt®, Nümbrecht, Germany) containing DMEM medium (Gibco™, 11965092) supplemented with 10% fetal calf serum (Gibco™, 10099141), penicillin (100 U/mL), and 1% L-glutamine, and cultured in an incubator at 37 °C, 5% CO_2.

4.3. Phage Display Biopanning

Cell-based phage display biopanning was performed following procedures previously described [40,41,81]. The scFv phage library used for the first round of biopanning was the Jones–Mahler human naïve library [40]. The rounds of biopanning alternated between CHO XL99 cells and HEK293 cells. GFP positive cells were sorted at the Queensland Brain Institute Flow Cytometry facility (UQ) using a BD FACSymphony™ S6 Cell Sorter (Franklin Lakes, NJ, USA).

4.4. Flow Cytometry Analysis of Phage Pools

CHO XL99 cells were transfected with the pEGFP-N1-mVCAM-1 plasmid (Supplementary Table S2) and grown for 24 h. The 10^{11} phages from the naïve phage display library or round 1 and round 2 amplified phage pools were diluted in 1.8 mL of 2% skim milk in PBS (MPBS) and incubated at 4 °C, rotating for 20 min. A total of 10^6 transfected and non-transfected CHO XL99 cells were harvested by centrifugation at 300× *g* for 5 min and washed with 1 mL of PBS. Next, cells were incubated with each diluted phage pool in MPBS for 1 h, rotating at 4 °C. Cells were washed 3 times with 1 mL PBS and were then incubated in a 1:200 dilution of mouse anti-M13 mAb (Sino Biological, Houston, TX, USA, Cat# 11973-MM05T, RRID:AB_2857926) in MPBS on ice for 1 h. Cells were harvested and washed twice with 1 mL PBS as above. Next, cells were incubated in a 1:400 dilution (1.25 µg/mL) of goat anti-mouse Dylight650 (Abcam, Cambridge, UK, Cat# ab96874, RRID:AB_10679531) in MPBS in the dark, on ice, for 1 h. Cells were harvested and washed 3 times in PBS as above, and gently resuspended in 100 µL 4% paraformaldehyde (PFA) in PBS. After incubation on ice for 15–20 min, cells were washed 3 times as above and resuspended in 200 µL of PBS prior to analysis by flow cytometry using a Beckman Coulter CytoFLEX S (Beckman Coulter Life Sciences, Mount Waverley, VIC, Australia).

4.5. Whole-Cell Phage Binding ELISA

Individual phage clones from the second biopanning round were tested for binding to cell surface expressed mVCAM-1 by whole-cell enzyme-linked immunosorbent assay (ELISA). The phage clones were prepared in a 96-well format as previously described [40,41], and were used for ELISA on 96-well plates coated with CHO-K1 cells expressing mVCAM-1-eGFP or eGFP alone (negative control). To coat the plates, transfected CHO-K1 cells were seeded onto 96-well plates to a density of 40,000 cells/well in 200 µL of F12K media supplemented with 10% FBS and penicillin-streptomycin antibiotic, and were incubated overnight at 37 °C, 7.5% CO_2. Next, cells were fixed in 4% PFA in PBS, and plates were left to dry at room temperature for 10 min. Phages and cells were separately blocked in MPBS for 1 h at room temperature, and then the blocked phages were added to the blocked cells and incubated for 1 h at room temperature. Plates were washed six times with PBS + 0.1% Tween 20 using a plate washer (BioTek, Agilent, Santa Clara, CA, USA, ELx405 Select). Next, a 1:5000 dilution of mouse anti-M13 monoclonal antibody (Sino Biological Cat# 11973-MM05T, RRID:AB_2857926) in MPBS was added to the wells, followed by 1 h room temperature incubation. Plates were washed as above, then incubated in a 1:5000 dilution in MPBS of goat anti-mouse IgG (H + L)-HRP conjugated secondary antibody (Bio-

Rad Cat# 1706516, RRID:AB_2921252) for 1 h at room temperature. After the final wash, plates were developed using TMB substrate (BioLegend, San Diego, CA, USA, 423001) following the manufacturer's instructions. Absorbance at 450 nm was measured using a microplate spectrometer (BioTek PowerWave XS2). The controls for this experiment included cells transfected with pEGFP-N1 empty vector and cells incubated only with primary and secondary antibodies but no phages. We considered an absorbance reading as positive if it complied with the following two rules: (1) the absorbance of the phage sample on VCAM-1-eGFP transfected cells was at least 4 times greater than the average signal of all the control wells in that same plate, and (2) the absorbance of the same phage sample on GFP-only transfected cells was below 2 times the value of the average of the control wells in the corresponding plate (Supplementary Figure S2).

4.6. Flow Cytometry Analysis of Selected Phages and Purified Antibodies

Flow cytometry was used to verify the binding of selected phages, purified scFv-LPETG clones, and purified mAbs to mVCAM-1-eGFP. To test the phages, CHO XL99 cells were transfected or not with pEGFP-N1-mVCAM-1, and 24–48 h later, cells were aliquoted into wells of a round bottomed 96-well plate (2.5×10^5 cells/well). Cells were pelleted by centrifugation at $300\times$ *g* for 5 min at room temperature, were washed with 200 µL of PBS, and were blocked with 25 µL of MPBS. The selected positive purified phages (30 µL) were blocked with 30 µL of 4% MPBS for 30 min at room temperature in a separate 96-well plate, and blocked phages were then combined with the blocked cells. After 1 h incubation at 4 °C, cells were washed with 200 µL of PBS and incubated in 50 µL of 1:200 anti-M13 antibody (Sino Biological Cat# 11973-MM05T, RRID:AB_2857926) for 1 h at 4 °C. Next, cells were washed 3 times with 200 µL PBS, and were incubated for 1 h at 4 °C in 50 µL of 1:400 (1.25 µg/mL) goat anti-mouse IgG Dylight650 (Abcam Cat# ab96874, RRID:AB_10679531). Cells were washed as above, fixed in 4% PFA in PBS, and analyzed by flow cytometry as described above for the polyclonal flow cytometry.

A similar protocol was used for the scFv-LPETGs, except that 1 µg scFv was used per 10,000 cells instead of phages, the primary antibody used was a 1:200 dilution (2.5 µg/mL) of purified mouse anti-6XHIS with control (BD Biosciences, Franklin Lakes, NJ, USA, Cat# 552565, RRID:AB_394432), and no fixing with PFA was necessary.

For the mAbs, a 1:3 mixture of non-transfected to transiently transfected ExpiCHO cells were collected by centrifugation at $300\times$ *g* for 5 min and blocked in ice-cold FACS-Block (3% fetal calf serum (FCS) (Gibco, A3160902), 0.1% bovine serum albumin (BSA) (Bovogen, Melbourne, Australia, SFBS-F), and 0.1% sodium azide) at a concentration of 1×10^6 cells/mL for 30 min. Next, cells were harvested by centrifugation and resuspended in ice-cold FACSWash buffer (0.2% FCS, 0.1% BSA, 0.1% sodium azide) at a concentration of 5×10^6 cells/mL, and 40,000 cells were aliquoted/well in a 96-V-shaped wells plate. The FACSWash buffer was removed by centrifugation at $400\times$ *g* for 5 min, and cells were resuspended in 50 µL of FACSWash containing 11.1 µg/mL of each reformatted anti-VCAM-1 antibody or isotype control mIgG2a (Miltenyi Biotec, Bergisch Gladbach, Germany, Cat# 130-106-546, RRID:AB_2661589), a 1:200 dilution (2.5 µg/mL) of rat anti-mouse VCAM-1 (Millipore, Burlington, MA, USA, Cat# CBL1300, RRID:AB_2214062), or 1:400 dilution of mouse IgG1 anti-FLAG (Cell Signaling Technology, Danvers, MA, USA, Cat# 8146, RRID:AB_10950495). For no antibody control wells, cells were incubated in FACSWash only. After 1 h incubation at 4 °C, cells were collected by centrifugation and washed 3 times with 150–200 µL of FACSWash, followed by a 30 min incubation at 4 °C in FACSWash containing 1:400 (1.25 µg/mL) goat IgG anti-mouse IgG H&L Dylight650 (Abcam Cat# ab96874, RRID:AB_10679531) or 1:200 (1 µg/mL) goat anti-rat-PE-Cy7 (BioLegend Cat# 405413, RRID:AB_10661733) antibodies, or FACSWash for no antibody controls. Next, cells were collected by centrifugation, washed 3 times in FACSWash, and resuspended in 100 µL of FACSWash supplemented with 0.25% PFA. Cells were analyzed by flow cytometry using a Beckman Coulter CytoFLEX S and the data collected were analyzed using CytExpert v2.4.0.28 and FlowJo v10.6.2 (FlowJo LLC, BD Biosciences, Franklin Lakes, NJ, USA). Me-

dian fluorescence intensity (MFI) was used as a measure of binding of the different mAbs to VCAM-1 and its Ig-like mutant versions.

4.7. Expression and Purification of scFv and Full-Length Antibodies

scFv-LPETG antibodies were expressed in SHuffle® Express *E. coli* cells (New England BioLabs® Inc., Ipswich, MA, USA). Overnight cultures of the SHuffle strains carrying the different pET28b-scFvs were diluted 1:100 in 200 mL TB medium (Merck, Darmstadt, Germany, T0918) supplemented with kanamycin (30 µg/mL) and were grown at 37 °C at 200 rpm until cells reached log phase (OD_{600} = 0.8–1.0). The culture was allowed to reach room temperature, and scFv-LPETG expression was induced by adding 1 mM of isopropyl β-D-1-thiogalactopyranoside (IPTG). Protein expression was conducted overnight at 25 °C, 200 rpm. Cells were harvested the following day by centrifugation at 5000× *g* for 10 min at room temperature. Bacterial pellets were resuspended in 30 mL of ice-cold equilibration buffer (20 mM sodium phosphate, 0.5 M NaCl, 20 mM imidazole, pH of 7.4) by vigorous pipetting, and were sonicated on ice (SONICS Ultrasonic Processor VC-505, Sonics & Materials Inc., Newtown, CT, USA) for 5 min (20% amplitude, pulse 1 s on 1 s off, 3 mm tip diameter). The lysate was incubated at 4 °C, rotating, for 1 h and then centrifuged in an Avanti JXN-30 (Beckman Coulter Inc., Brea, CA, USA) at 18,000× *g* for 30 min at 4 °C. The supernatant was recentrifuged at 20,000× *g* for 30 min at 4 °C, transferred to a pre-cooled vessel, and the scFv-LPETGs were purified using the Äkta Explorer fast protein liquid chromatography (FPLC) system using a 1 mL HisTrap column (HisTrap™ High Performance, Cytiva, Marlborough, MA, USA, 17524701), and the following standard procedures. The scFv-LPETG clones were eluted in elution buffer (20 mM sodium phosphate, 0.5 M NaCl, 400 mM imidazole, pH of 7.4) on ice and dialyzed in 14 kDa cutoff dialysis tubing against a solution of 1X PBS overnight at 4 °C. The pH of the dialysis buffer was adjusted to 1 unit above the theoretical pI of each scFv (Supplementary Table S4). The dialyzed samples were concentrated using a centrifugal concentrator (Vivaspin® 6 Centrifugal Concentrator, VS0602, Sartorius, Göttingen, Germany) with a 10 kDa Molecular weight cut-off (MWCO) by centrifuging at 4000× *g* at 4 °C. The concentration of scFv-LPETG was determined with a Nanodrop Spectrophotometer (Thermo Fisher Scientific, Waltham, MA USA), considering the calculated extinction coefficients (Supplementary Table S4). Samples were transferred to 1.5 mL Protein LoBind® tubes (Eppendorf, Hamburg, Germany, 0030108442) and stored at 4 °C for the short term or supplemented with 10% *v*/*v* final concentration of glycerol, frozen in liquid nitrogen, and stored long term at −80 °C.

mAbs were expressed as previously described [41] using ExpiCHO cells and the high titer protocol from the ExpiFectamine CHO Transfection kit (Thermo Fisher, A29131). The supernatant was loaded into a prepacked HiTrap MabSelect column (Cytiva, 28408253) and purified using an Äkta Explorer FPLC system. Purified mAbs were buffer exchanged and concentrated using Amicon Ultra Centrifugal filters and stored in 10% glycerol, PBS pH of 7.4 at −80 °C until use.

4.8. SDS-PAGE and Western Blotting

The presence of antibodies in the supernatant and eluates was determined using sodium dodecyl sulphate–polyacrylamide gel electrophoresis (SDS-PAGE) as follows. For scFv-LPETGs, 5 µg of each purified antibody samples were mixed with 4X NuPAGE loading buffer supplemented with 10 mM DTT, heated at 95 °C for 5 min, centrifuged for 1 min at 21,000× *g*, and loaded in 10% acrylamide gels (Bio-Rad, 4561033). Protein detection was achieved by either staining the gel with SimplyBlue™ SafeStain (LC6065) following the manufacturer's protocol, or by Western blot. For purified mAbs, 5 µg of each purified antibody was resuspended on 4X SDS-PAGE loading buffer (200 mM Tris-HCl pH of 6.8, 8% SDS, 0.4% bromophenol blue, 40% glycerol) supplemented or not with a final concentration of 10 mM DTT. The sample was heated at 95 °C for 5 min, centrifuged for 1 min at 21,000× *g*, and separated in a 4–15% stain-free gel (BioRad, 4568081). All gels were visualized on a BioRad Chemidoc imaging system.

For Western blotting, proteins were transferred from acrylamide gels into a polyvinylidene fluoride (PVDF) membrane using the BioRad Trans-Blot Turbo RTA Transfer Kit (1704272) and a Trans-Blot Turbo Transfer system (7 min at 1.3 A), following the manufacturer's protocol. The membrane was blocked with 5% skim milk in Tris-buffered saline (50 mM Tris-Cl, pH of 7.5, 150 mM NaCl) with 0.1% Tween 20 (TBS-T) for 1 h at room temperature, rocking. The membrane was then incubated with a 1:5000 dilution of anti-His-HRP (Miltenyi Biotec Cat# 130-092-785, RRID:AB_1103231) in 2% skim milk TBS-T overnight, rocking at 4 °C. After 3 washes with TBS-T for 5 min at room temperature, membranes were developed with the Super signal West Dura Extended Duration Substrate kit (ThermoFisher Scientific, 34075) and visualized in the BioRad ChemiDoc gel imaging system.

4.9. Bioinformatic Analysis of scFv Sequences

To identify variable domains of immunoglobulins in the scFv sequences, we used IgBlast (IgBlast tool (nih.gov)) from the National Centre for Biotechnology Information (NCBI)). To annotate the variable regions with the ImMunoGeneTics (IMGT) numbering system, we used the Antigen receptor Numbering and Receptor Classification (ANARCI) by SAbPred (http://opig.stats.ox.ac.uk/webapps/newsabdab/sabpred/anarci/ (accessed on 5 June 2021)). The molecular weight, extinction coefficient, and theoretical pI for each scFv-LPETG (Supplementary Table S4) were calculated using ProtParam (ExPASy–ProtParam tool) based on the scFv's amino acid sequences. Amino acid sequences were aligned using Clustal Omega (https://www.ebi.ac.uk/Tools/msa/clustalo/ (accessed on 5 June 2021)), which was also used to generate phylogenetic trees.

4.10. In Vitro Cell Adhesion Assay

SVEC4-10 endothelial cells were seeded into a 96-well plate at a density of 10,000 cells/well and incubated for 24 h. The cells were then separately treated with 100 ng/mL lipopolysaccharide (LPS) (Sigma-Aldrich, Burlington, MA, USA, L2630) for 24 h. J774A.1 macrophages were stained on the same day with 25 ng/mL of DiOC6 for 24 h at 37 °C. After 24 h LPS stimulation, SVEC4-10 endothelial cells were treated with the following different antibodies at a concentration of 20 µg/mL, for 1 h at 37 °C: rat anti-VCAM-1 (Millipore Cat# CBL1300, RRID:AB_2214062) was used as positive control; a random scFv (not mVCAM-1 binder, a kind gift from the National Biologics Facility, UQ) was used as negative control; and 6 different purified scFv-LPETG antibodies from this work (1A9, 2D3, 2D8, 2E2, 2E6, and 3H4). After incubation, endothelial cells were washed once with PBS. The DiOC6-labelled J774A.1 cells were detached by washing with PBS and centrifuged at 500× *g* for 5 min, followed by resuspension in DMEM, high glucose medium (Cat #11965-092, Thermo Fisher) supplemented with 10% fetal bovine serum (Cat #26140079, Thermo Fisher) and 1% penicillin-streptomycin (Cat #15140122, Thermo Fisher). Next, DiOC6-labelled J774A.1 cells were added to SVEC4-10 endothelial cells at a density of 10,000 cells/well. After 10 min of coculture treatment, all wells were washed once with PBS and then fixed with 4% PFA in PBS for analysis. Fluorescent images were taken with an OLYMPUS CKX53 fluorescent microscope (Olympus, Tokyo, Japan) with the Cool LED pE-300 light source and OLYMPUS-DP74 camera. The relative fluorescent intensity was quantified with ImageJ v1.53t. The experiment was performed twice with four or five replicates/group, for a total of 9.

4.11. Statistical Analysis of Data

Data are presented as mean +/− standard error unless specified in the figure legend. One-way ANOVA followed by post-hoc Tukey test for pairwise comparisons was used in the analysis of significant differences in the cell adhesion assay. A p value < 0.05 was considered significant. Graphs were plotted using GraphPad Prism 10.

Supplementary Materials: The following supporting information can be downloaded at: https://www.mdpi.com/article/10.3390/ijms252413650/s1. References [82–86] are cited in the supplementary materials.

Author Contributions: Conceptualization, H.T.T. and L.F.Z.; data curation, B.P. and L.F.Z.; formal analysis, B.P., Y.W. and L.F.Z.; funding acquisition, M.L.J., H.T.T. and L.F.Z.; investigation, B.P., J.R.P., Y.W., F.M.B. and L.F.Z.; methodology, Y.W., N.P., C.F., D.P.S., M.L.J., H.T.T. and L.F.Z.; project administration, L.F.Z.; resources, M.L.J., H.T.T. and L.F.Z.; supervision, H.T.T. and L.F.Z.; writing—original draft, B.P., Y.W., F.M.B. and L.F.Z.; writing—review and editing, B.P., C.F., D.P.S., M.L.J., H.T.T. and L.F.Z. All authors have read and agreed to the published version of the manuscript.

Funding: This work was funded by a Heart Foundation Future Leader Fellowship to H.T.T., an Australian Research Council Industrial Transformation Training Centre IC160100027 to M.L.J., and a Promoting Women Fellowship from the University of Queensland to L.F.Z. Elements of this research utilized the facilities and resources of the National Biologics Facility (NBF), University of Queensland. NBF is supported by Therapeutic Innovation Australia (TIA). TIA is supported by the Australian Government through the National Collaborative Research Infrastructure Strategy (NCRIS) program.

Institutional Review Board Statement: Not applicable.

Informed Consent Statement: Not applicable.

Data Availability Statement: The raw data supporting the conclusions of this article will be made available by the authors on request. Antibody sequences will not be made available to protect commercialization potential.

Acknowledgments: We thank Zhao Wang from the Rowan lab at The University of Queensland for the confocal microscopy images, and Christopher Howard for his help with protein purification.

Conflicts of Interest: The authors declare no conflicts of interest.

References

1. Pickett, J.R.; Wu, Y.; Zacchi, L.F.; Ta, H.T. Targeting endothelial vascular cell adhesion molecule-1 in atherosclerosis: Drug discovery and development of vascular cell adhesion molecule-1-directed novel therapeutics. *Cardiovasc. Res.* **2023**, *119*, 2278–2293. [CrossRef] [PubMed]
2. Cook-Mills, J.M.; Marchese, M.E.; Abdala-Valencia, H. Vascular cell adhesion molecule-1 expression and signaling during disease: Regulation by reactive oxygen species and antioxidants. *Antioxid. Redox Signal* **2011**, *15*, 1607–1638. [CrossRef]
3. Kong, D.H.; Kim, Y.K.; Kim, M.R.; Jang, J.H.; Lee, S. Emerging Roles of Vascular Cell Adhesion Molecule-1 (VCAM-1) in Immunological Disorders and Cancer. *Int. J. Mol. Sci.* **2018**, *19*, 1057. [CrossRef]
4. Galkina, E.; Ley, K. Vascular adhesion molecules in atherosclerosis. *Arterioscler. Thromb. Vasc. Biol.* **2007**, *27*, 2292–2301. [CrossRef] [PubMed]
5. Minn, A.J.; Gupta, G.P.; Siegel, P.M.; Bos, P.D.; Shu, W.; Giri, D.D.; Viale, A.; Olshen, A.B.; Gerald, W.L.; Massague, J. Genes that mediate breast cancer metastasis to lung. *Nature* **2005**, *436*, 518–524. [CrossRef] [PubMed]
6. Kim, M.R.; Jang, J.H.; Park, C.S.; Kim, T.K.; Kim, Y.J.; Chung, J.; Shim, H.; Nam, I.H.; Han, J.M.; Lee, S. A Human Antibody That Binds to the Sixth Ig-Like Domain of VCAM-1 Blocks Lung Cancer Cell Migration In Vitro. *Int. J. Mol. Sci.* **2017**, *18*, 566. [CrossRef] [PubMed]
7. Siyasi, M.; Mahjoubi, F.; Mahjoubi, B.; Shabani, S. Study of VCAM-1 gene expression in normal and tumoral tissues in patients with colorectal cancer. *J. Biotechnol. Biomed. Sci.* **2017**, *1*, 19–26. [CrossRef]
8. Hession, C.; Tizard, R.; Vassallo, C.; Schiffer, S.B.; Goff, D.; Moy, P.; Chi-Rosso, G.; Luhowskyj, S.; Lobb, R.; Osborn, L. Cloning of an alternate form of vascular cell adhesion molecule-1 (VCAM1). *J. Biol. Chem.* **1991**, *266*, 6682–6685. [CrossRef] [PubMed]
9. Taichman, D.B.; Cybulsky, M.I.; Djaffar, I.; Longenecker, B.M.; Teixido, J.; Rice, G.E.; Aruffo, A.; Bevilacqua, M.P. Tumor cell surface alpha 4 beta 1 integrin mediates adhesion to vascular endothelium: Demonstration of an interaction with the N-terminal domains of INCAM-110/VCAM-1. *Cell Regul.* **1991**, *2*, 347–355. [CrossRef] [PubMed]
10. Elices, M.J.; Osborn, L.; Takada, Y.; Crouse, C.; Luhowskyj, S.; Hemler, M.E.; Lobb, R.R. VCAM-1 on activated endothelium interacts with the leukocyte integrin VLA-4 at a site distinct from the VLA-4/fibronectin binding site. *Cell* **1990**, *60*, 577–584. [CrossRef] [PubMed]
11. Rao, S.P.; Wang, Z.; Zuberi, R.I.; Sikora, L.; Bahaie, N.S.; Zuraw, B.L.; Liu, F.T.; Sriramarao, P. Galectin-3 functions as an adhesion molecule to support eosinophil rolling and adhesion under conditions of flow. *J. Immunol.* **2007**, *179*, 7800–7807. [CrossRef] [PubMed]
12. Kelly, K.A.; Allport, J.R.; Yu, A.M.; Sinh, S.; Sage, E.H.; Gerszten, R.E.; Weissleder, R. SPARC is a VCAM-1 counter-ligand that mediates leukocyte transmigration. *J. Leukoc. Biol.* **2007**, *81*, 748–756. [CrossRef] [PubMed]

13. Rao, S.P.; Ge, X.N.; Sriramarao, P. Regulation of Eosinophil Recruitment and Activation by Galectins in Allergic Asthma. *Front. Med.* **2017**, *4*, 68. [CrossRef] [PubMed]
14. Troncoso, M.F.; Elola, M.T.; Blidner, A.G.; Sarrias, L.; Espelt, M.V.; Rabinovich, G.A. The universe of galectin-binding partners and their functions in health and disease. *J. Biol. Chem.* **2023**, *299*, 105400. [CrossRef] [PubMed]
15. Baiula, M.; Spampinato, S.; Gentilucci, L.; Tolomelli, A. Novel Ligands Targeting $\alpha_4\beta_1$ Integrin: Therapeutic Applications and Perspectives. *Front. Chem.* **2019**, *7*, 489. [CrossRef] [PubMed]
16. Wittchen, E.S. Endothelial signaling in paracellular and transcellular leukocyte transmigration. *Front. Biosci. (Landmark Ed.)* **2009**, *14*, 2522–2545. [CrossRef] [PubMed]
17. van Wetering, S.; van den Berk, N.; van Buul, J.D.; Mul, F.P.; Lommerse, I.; Mous, R.; ten Klooster, J.P.; Zwaginga, J.J.; Hordijk, P.L. VCAM-1-mediated Rac signaling controls endothelial cell-cell contacts and leukocyte transmigration. *Am. J. Physiol. Cell Physiol.* **2003**, *285*, C343–C352. [CrossRef]
18. Cybulsky, M.I.; Fries, J.W.; Williams, A.J.; Sultan, P.; Eddy, R.; Byers, M.; Shows, T.; Gimbrone, M.A., Jr.; Collins, T. Gene structure, chromosomal location, and basis for alternative mRNA splicing of the human VCAM1 gene. *Proc. Natl. Acad. Sci. USA* **1991**, *88*, 7859–7863. [CrossRef] [PubMed]
19. Hession, C.; Moy, P.; Tizard, R.; Chisholm, P.; Williams, C.; Wysk, M.; Burkly, L.; Miyake, K.; Kincade, P.; Lobb, R. Cloning of murine and rat vascular cell adhesion molecule-1. *Biochem. Biophys. Res. Commun.* **1992**, *183*, 163–169. [CrossRef] [PubMed]
20. Cybulsky, M.I.; Fries, J.W.; Williams, A.J.; Sultan, P.; Davis, V.M.; Gimbrone, M.A., Jr.; Collins, T. Alternative splicing of human VCAM-1 in activated vascular endothelium. *Am. J. Pathol.* **1991**, *138*, 815–820. [PubMed]
21. Woodside, D.G.; Kram, R.M.; Mitchell, J.S.; Belsom, T.; Billard, M.J.; McIntyre, B.W.; Vanderslice, P. Contrasting roles for domain 4 of VCAM-1 in the regulation of cell adhesion and soluble VCAM-1 binding to integrin alpha4beta1. *J. Immunol.* **2006**, *176*, 5041–5049. [CrossRef] [PubMed]
22. Black, R.A. Tumor necrosis factor-alpha converting enzyme. *Int. J. Biochem. Cell Biol.* **2002**, *34*, 1–5. [CrossRef]
23. Garton, K.J.; Gough, P.J.; Philalay, J.; Wille, P.T.; Blobel, C.P.; Whitehead, R.H.; Dempsey, P.J.; Raines, E.W. Stimulated shedding of vascular cell adhesion molecule 1 (VCAM-1) is mediated by tumor necrosis factor-alpha-converting enzyme (ADAM 17). *J. Biol. Chem.* **2003**, *278*, 37459–37464. [CrossRef] [PubMed]
24. Troncoso, M.F.; Ortiz-Quintero, J.; Garrido-Moreno, V.; Sanhueza-Olivares, F.; Guerrero-Moncayo, A.; Chiong, M.; Castro, P.F.; Garcia, L.; Gabrielli, L.; Corbalan, R.; et al. VCAM-1 as a predictor biomarker in cardiovascular disease. *Biochim. Biophys. Acta Mol. Basis Dis.* **2021**, *1867*, 166170. [CrossRef] [PubMed]
25. Wang, L.; Ding, Y.; Guo, X.; Zhao, Q. Role and mechanism of vascular cell adhesion molecule-1 in the development of rheumatoid arthritis. *Exp. Ther. Med.* **2015**, *10*, 1229–1233. [CrossRef]
26. Wellicome, S.M.; Kapahi, P.; Mason, J.C.; Lebranchu, Y.; Yarwood, H.; Haskard, D.O. Detection of a circulating form of vascular cell adhesion molecule-1: Raised levels in rheumatoid arthritis and systemic lupus erythematosus. *Clin. Exp. Immunol.* **1993**, *92*, 412–418. [CrossRef]
27. Vonderheide, R.H.; Springer, T.A. Lymphocyte adhesion through very late antigen 4: Evidence for a novel binding site in the alternatively spliced domain of vascular cell adhesion molecule 1 and an additional alpha 4 integrin counter-receptor on stimulated endothelium. *J. Exp. Med.* **1992**, *175*, 1433–1442. [CrossRef] [PubMed]
28. Osborn, L.; Vassallo, C.; Benjamin, C.D. Activated endothelium binds lymphocytes through a novel binding site in the alternately spliced domain of vascular cell adhesion molecule-1. *J. Exp. Med.* **1992**, *176*, 99–107. [CrossRef]
29. Renz, M.E.; Chiu, H.H.; Jones, S.; Fox, J.; Kim, K.J.; Presta, L.G.; Fong, S. Structural requirements for adhesion of soluble recombinant murine vascular cell adhesion molecule-1 to alpha 4 beta 1. *J. Cell Biol.* **1994**, *125*, 1395–1406. [CrossRef]
30. Newham, P.; Craig, S.E.; Seddon, G.N.; Schofield, N.R.; Rees, A.; Edwards, R.M.; Jones, E.Y.; Humphries, M.J. Alpha4 integrin binding interfaces on VCAM-1 and MAdCAM-1. Integrin binding footprints identify accessory binding sites that play a role in integrin specificity. *J. Biol. Chem.* **1997**, *272*, 19429–19440. [CrossRef] [PubMed]
31. Kim, T.K.; Park, C.S.; Na, H.J.; Lee, K.; Yoon, A.; Chung, J.; Lee, S. Ig-like domain 6 of VCAM-1 is a potential therapeutic target in TNFalpha-induced angiogenesis. *Exp. Mol. Med.* **2017**, *49*, e294. [CrossRef]
32. Lee, S.; Yoon, I.H.; Yoon, A.; Cook-Mills, J.M.; Park, C.G.; Chung, J. An antibody to the sixth Ig-like domain of VCAM-1 inhibits leukocyte transendothelial migration without affecting adhesion. *J. Immunol.* **2012**, *189*, 4592–4601. [CrossRef]
33. Lee, J.H.; Sohn, J.H.; Ryu, S.Y.; Hong, C.S.; Moon, K.D.; Park, J.W. A novel human anti-VCAM-1 monoclonal antibody ameliorates airway inflammation and remodelling. *J. Cell Mol. Med.* **2013**, *17*, 1271–1281. [CrossRef]
34. Park, J.G.; Ryu, S.Y.; Jung, I.H.; Lee, Y.H.; Kang, K.J.; Lee, M.R.; Lee, M.N.; Sonn, S.K.; Lee, J.H.; Lee, H.; et al. Evaluation of VCAM-1 antibodies as therapeutic agent for atherosclerosis in apolipoprotein E-deficient mice. *Atherosclerosis* **2013**, *226*, 356–363. [CrossRef] [PubMed]
35. Zhang, L.; Xue, S.; Ren, F.; Huang, S.; Zhou, R.; Wang, Y.; Zhou, C.; Li, Z. An atherosclerotic plaque-targeted single-chain antibody for MR/NIR-II imaging of atherosclerosis and anti-atherosclerosis therapy. *J. Nanobiotechnol.* **2021**, *19*, 296. [CrossRef] [PubMed]
36. Corroyer-Dulmont, A.; Valable, S.; Falzone, N.; Frelin-Labalme, A.M.; Tietz, O.; Toutain, J.; Soto, M.S.; Divoux, D.; Chazalviel, L.; Peres, E.A.; et al. VCAM-1 targeted alpha-particle therapy for early brain metastases. *Neuro Oncol.* **2020**, *22*, 357–368. [CrossRef]
37. Leavy, O. The birth of monoclonal antibodies. *Nat. Immunol.* **2016**, *17*, S13. [CrossRef]
38. Breedveld, F.C. Therapeutic monoclonal antibodies. *Lancet* **2000**, *355*, 735–740. [CrossRef] [PubMed]

39. Zhao, A.; Tohidkia, M.R.; Siegel, D.L.; Coukos, G.; Omidi, Y. Phage antibody display libraries: A powerful antibody discovery platform for immunotherapy. *Crit. Rev. Biotechnol.* **2016**, *36*, 276–289. [CrossRef]
40. Jones, M.L.; Alfaleh, M.A.; Kumble, S.; Zhang, S.; Osborne, G.W.; Yeh, M.; Arora, N.; Hou, J.J.; Howard, C.B.; Chin, D.Y.; et al. Targeting membrane proteins for antibody discovery using phage display. *Sci. Rep.* **2016**, *6*, 26240. [CrossRef] [PubMed]
41. Panagides, N.; Zacchi, L.F.; De Souza, M.J.; Morales, R.A.V.; Karnowski, A.; Liddament, M.T.; Owczarek, C.M.; Mahler, S.M.; Panousis, C.; Jones, M.L.; et al. Evaluation of Phage Display Biopanning Strategies for the Selection of Anti-Cell Surface Receptor Antibodies. *Int. J. Mol. Sci.* **2022**, *23*, 8470. [CrossRef]
42. Tsuruta, L.R.; dos Lopes, M.; Moro, A.M. Display Technologies for the Selection of Monoclonal Antibodies for Clinical Use. In *Antibody Engineering*; Intechopen: London, UK, 2018. [CrossRef]
43. Sioud, M. Phage Display Libraries: From Binders to Targeted Drug Delivery and Human Therapeutics. *Mol. Biotechnol.* **2019**, *61*, 286–303. [CrossRef] [PubMed]
44. Jones, M.L.; Mahler, S.M.; Kumble, S. Selection of Antibodies to Transiently Expressed Membrane Proteins Using Phage Display. In *Antibody Engineering: Methods and Protocols*; Nevoltris, D., Chames, P., Eds.; Springer: New York, NY, USA, 2018; pp. 179–195. [CrossRef]
45. D'Angelo, S.; Ferrara, F.; Naranjo, L.; Erasmus, M.F.; Hraber, P.; Bradbury, A.R.M. Many Routes to an Antibody Heavy-Chain CDR3: Necessary, Yet Insufficient, for Specific Binding. *Front. Immunol.* **2018**, *9*, 395. [CrossRef] [PubMed]
46. Ta, H.T.; Peter, K.; Hagemeyer, C.E. Enzymatic antibody tagging: Toward a universal biocompatible targeting tool. *Trends Cardiovasc. Med.* **2012**, *22*, 105–111. [CrossRef] [PubMed]
47. Ta, H.T.; Prabhu, S.; Leitner, E.; Jia, F.; von Elverfeldt, D.; Jackson, K.E.; Heidt, T.; Nair, A.K.; Pearce, H.; von Zur Muhlen, C.; et al. Enzymatic single-chain antibody tagging: A universal approach to targeted molecular imaging and cell homing in cardiovascular disease. *Circ. Res.* **2011**, *109*, 365–373. [CrossRef]
48. Carlos, T.M.; Schwartz, B.R.; Kovach, N.L.; Yee, E.; Rosa, M.; Osborn, L.; Chi-Rosso, G.; Newman, B.; Lobb, R.; Harlan, J.M. Vascular cell adhesion molecule-1 mediates lymphocyte adherence to cytokine-activated cultured human endothelial cells. *Blood* **1990**, *76*, 965–970. [CrossRef]
49. Rice, G.E.; Bevilacqua, M.P. An inducible endothelial cell surface glycoprotein mediates melanoma adhesion. *Science* **1989**, *246*, 1303–1306. [CrossRef] [PubMed]
50. Pepinsky, B.; Hession, C.; Chen, L.L.; Moy, P.; Burkly, L.; Jakubowski, A.; Chow, E.P.; Benjamin, C.; Chi-Rosso, G.; Luhowskyj, S.; et al. Structure/function studies on vascular cell adhesion molecule-1. *J. Biol. Chem.* **1992**, *267*, 17820–17826. [CrossRef]
51. Miyake, K.; Medina, K.; Ishihara, K.; Kimoto, M.; Auerbach, R.; Kincade, P.W. A VCAM-like adhesion molecule on murine bone marrow stromal cells mediates binding of lymphocyte precursors in culture. *J. Cell Biol.* **1991**, *114*, 557–565. [CrossRef] [PubMed]
52. Miyake, K.; Weissman, I.L.; Greenberger, J.S.; Kincade, P.W. Evidence for a role of the integrin VLA-4 in lympho-hemopoiesis. *J. Exp. Med.* **1991**, *173*, 599–607. [CrossRef]
53. Gorcyznski, R.M.; Chung, S.; Fu, X.M.; Levy, G.; Sullivan, B.; Chen, Z. Manipulation of skin graft rejection in alloimmune mice by anti-VCAM-1:VLA-4 but not anti-ICAM-1:LFA-1 monoclonal antibodies. *Transpl. Immunol.* **1995**, *3*, 55–61. [CrossRef] [PubMed]
54. Qiu, Z.Y.; Yu, W.J.; Bai, J.; Lin, Q.Y. Blocking VCAM-1 ameliorates hypertensive cardiac remodeling by impeding macrophage infiltration. *Front. Pharmacol.* **2022**, *13*, 1058268. [CrossRef]
55. Graber, N.; Gopal, T.V.; Wilson, D.; Beall, L.D.; Polte, T.; Newman, W. T cells bind to cytokine-activated endothelial cells via a novel, inducible sialoglycoprotein and endothelial leukocyte adhesion molecule-1. *J. Immunol.* **1990**, *145*, 819–830. [CrossRef] [PubMed]
56. Bochner, B.S.; Luscinskas, F.W.; Gimbrone, M.A., Jr.; Newman, W.; Sterbinsky, S.A.; Derse-Anthony, C.P.; Klunk, D.; Schleimer, R.P. Adhesion of human basophils, eosinophils, and neutrophils to interleukin 1-activated human vascular endothelial cells: Contributions of endothelial cell adhesion molecules. *J. Exp. Med.* **1991**, *173*, 1553–1557. [CrossRef]
57. Damle, N.K.; Aruffo, A. Vascular cell adhesion molecule 1 induces T-cell antigen receptor-dependent activation of CD4+T lymphocytes. *Proc. Natl. Acad. Sci. USA* **1991**, *88*, 6403–6407. [CrossRef]
58. Zohlnhofer, D.; Brand, K.; Schipek, K.; Pogatsa-Murray, G.; Schomig, A.; Neumann, F.J. Adhesion of monocyte very late antigen-4 to endothelial vascular cell adhesion molecule-1 induces interleukin-1beta-dependent expression of interleukin-6 in endothelial cells. *Arterioscler. Thromb. Vasc. Biol.* **2000**, *20*, 353–359. [CrossRef]
59. Rice, G.E.; Munro, J.M.; Bevilacqua, M.P. Inducible cell adhesion molecule 110 (INCAM-110) is an endothelial receptor for lymphocytes. A CD11/CD18-independent adhesion mechanism. *J. Exp. Med.* **1990**, *171*, 1369–1374. [CrossRef]
60. Sriramarao, P.; DiScipio, R.G.; Cobb, R.R.; Cybulsky, M.; Stachnick, G.; Castaneda, D.; Elices, M.; Broide, D.H. VCAM-1 is more effective than MAdCAM-1 in supporting eosinophil rolling under conditions of shear flow. *Blood* **2000**, *95*, 592–601. [CrossRef]
61. Ross, E.A.; Douglas, M.R.; Wong, S.H.; Ross, E.J.; Curnow, S.J.; Nash, G.B.; Rainger, E.; Scheel-Toellner, D.; Lord, J.M.; Salmon, M.; et al. Interaction between integrin alpha9beta1 and vascular cell adhesion molecule-1 (VCAM-1) inhibits neutrophil apoptosis. *Blood* **2006**, *107*, 1178–1183. [CrossRef] [PubMed]
62. Hakugawa, J.; Bae, S.J.; Tanaka, Y.; Katayama, I. The inhibitory effect of anti-adhesion molecule antibodies on eosinophil infiltration in cutaneous late phase response in Balb/c mice sensitized with ovalbumin (OVA). *J. Dermatol.* **1997**, *24*, 73–79. [CrossRef]

63. Dudgeon, T.J.; Bottomley, M.J.; Driscoll, P.C.; Humphries, M.J.; Mould, A.P.; Wingfield, G.I.; Clements, J.M. Expression and characterisation of a very-late antigen-4 (alpha 4 beta 1) integrin-binding fragment of vascular cell-adhesion molecule-1. *Eur. J. Biochem.* **1994**, *226*, 517–523. [CrossRef] [PubMed]
64. Patel, K.D. Eosinophil tethering to interleukin-4-activated endothelial cells requires both P-selectin and vascular cell adhesion molecule-1. *Blood* **1998**, *92*, 3904–3911. [CrossRef] [PubMed]
65. Zacchi, L.F.; Schulz, B.L. N-glycoprotein macroheterogeneity: Biological implications and proteomic characterization. *Glycoconj. J.* **2016**, *33*, 359–376. [CrossRef] [PubMed]
66. Lu, R.M.; Hwang, Y.C.; Liu, I.J.; Lee, C.C.; Tsai, H.Z.; Li, H.J.; Wu, H.C. Development of therapeutic antibodies for the treatment of diseases. *J. Biomed. Sci.* **2020**, *27*, 1. [CrossRef] [PubMed]
67. Alfaleh, M.A.; Arora, N.; Yeh, M.; de Bakker, C.J.; Howard, C.B.; Macpherson, P.; Allavena, R.E.; Chen, X.; Harkness, L.; Mahler, S.M.; et al. Canine CD117-Specific Antibodies with Diverse Binding Properties Isolated from a Phage Display Library Using Cell-Based Biopanning. *Antibodies* **2019**, *8*, 15. [CrossRef]
68. Alfaleh, M.A.; Jones, M.L.; Howard, C.B.; Mahler, S.M. Strategies for Selecting Membrane Protein-Specific Antibodies using Phage Display with Cell-Based Panning. *Antibodies* **2017**, *6*, 10. [CrossRef] [PubMed]
69. Askew, R.L.; Cook, K.F.; Keefe, F.J.; Nowinski, C.J.; Cella, D.; Revicki, D.A.; Morgan DeWitt, E.M.; Michaud, K.; Trence, D.L.; Amtmann, D. A PROMIS Measure of Neuropathic Pain Quality. *Value Health* **2016**, *19*, 623–630. [CrossRef] [PubMed]
70. Lorenzon, P.; Vecile, E.; Nardon, E.; Ferrero, E.; Harlan, J.M.; Tedesco, F.; Dobrina, A. Endothelial cell E- and P-selectin and vascular cell adhesion molecule-1 function as signaling receptors. *J. Cell Biol.* **1998**, *142*, 1381–1391. [CrossRef]
71. Bates, A.; Power, C.A. David vs. Goliath: The Structure, Function, and Clinical Prospects of Antibody Fragments. *Antibodies* **2019**, *8*, 28. [CrossRef]
72. Muñoz-López, P.; Ribas-Aparicio, R.M.; Becerra-Báez, E.I.; Fraga-Pérez, K.; Flores-Martínez, L.F.; Mateos-Chávez, A.A.; Luria-Pérez, R. Single-Chain Fragment Variable: Recent Progress in Cancer Diagnosis and Therapy. *Cancers* **2022**, *14*, 4206. [CrossRef] [PubMed]
73. Satheeshkumar, P.K. Expression of Single Chain Variable Fragment (scFv) Molecules in Plants: A Comprehensive Update. *Mol. Biotechnol.* **2020**, *62*, 151–167. [CrossRef] [PubMed]
74. Nilvebrant, J.; Tessier, P.M.; Sidhu, S.S. Engineered Autonomous Human Variable Domains. *Curr. Pharm. Des.* **2016**, *22*, 6527–6537. [CrossRef] [PubMed]
75. Monnier, P.P.; Vigouroux, R.J.; Tassew, N.G. In Vivo Applications of Single Chain Fv (Variable Domain) (scFv) Fragments. *Antibodies* **2013**, *2*, 193–208. [CrossRef]
76. Wan, L.; Zhu, S.; Zhu, J.; Yang, H.; Li, S.; Li, Y.; Cheng, J.; Lu, X. Production and characterization of a CD25-specific scFv-Fc antibody secreted from Pichia pastoris. *Appl. Microbiol. Biotechnol.* **2013**, *97*, 3855–3863. [CrossRef]
77. Yokota, T.; Milenic, D.E.; Whitlow, M.; Schlom, J. Rapid tumor penetration of a single-chain Fv and comparison with other immunoglobulin forms. *Cancer Res.* **1992**, *52*, 3402–3408. [PubMed]
78. Garousi, J.; Orlova, A.; Frejd, F.Y.; Tolmachev, V. Imaging using radiolabelled targeted proteins: Radioimmunodetection and beyond. *EJNMMI Radiopharm. Chem.* **2020**, *5*, 16. [CrossRef] [PubMed]
79. Huang, L.; Su, X.; Federoff, H.J. Single-chain fragment variable passive immunotherapies for neurodegenerative diseases. *Int. J. Mol. Sci.* **2013**, *14*, 19109–19127. [CrossRef]
80. Jones, M.L.; Seldon, T.; Smede, M.; Linville, A.; Chin, D.Y.; Barnard, R.; Mahler, S.M.; Munster, D.; Hart, D.; Gray, P.P.; et al. A method for rapid, ligation-independent reformatting of recombinant monoclonal antibodies. *J. Immunol. Methods* **2010**, *354*, 85–90. [CrossRef]
81. Lee, C.M.; Iorno, N.; Sierro, F.; Christ, D. Selection of human antibody fragments by phage display. *Nat. Protoc.* **2007**, *2*, 3001–3008. [CrossRef]
82. Bazan, J.; Calkosinski, I.; Gamian, A. Phage display—A powerful technique for immunotherapy: 1. Introduction and potential of therapeutic application. *Hum. Vaccin Immunother.* **2012**, *8*, 1817–1828. [CrossRef]
83. Bashir, S.; Paeshuyse, J. Construction of Antibody Phage Libraries and Their Application in Veterinary Immunovirology. *Antibodies* **2020**, *9*, 21. [CrossRef]
84. Lim, C.C.; Woo, P.C.Y.; Lim, T.S. Development of a Phage Display Panning Strategy Utilizing Crude Antigens: Isolation of MERS-CoV Nucleoprotein human antibodies. *Sci. Rep.* **2019**, *9*, 6088. [CrossRef]
85. Ma, H.; O'Kennedy, R. Recombinant antibody fragment production. *Methods* **2019**, *116*, 23–33. [CrossRef]
86. Reparon-Schuijt, C.C.; Van Esch, W.J.; Van Kooten, C.; Rozier, B.C.; Levarht, E.W.; Breedveld, F.C.; Verweij, C.L. Regulation of synovial B cell survival in rheumatoid arthritis by vascular cell adhesion molecule 1 (CD106) expressed on fibroblast-like synoviocytes. *Arthritis Rheum.* **2000**, *43*, 1115–1121. [CrossRef]

Supplementary information

General information on phage display biopanning

Phage display antibody biopanning requires the generation of an antibody library fused to a phage coat protein that is expressed on the surface of the phage [1, 2]. To construct a phage display library, the gene fragments encoding the variable regions of the heavy and light chains of antibodies are extracted from the mRNA of B cells from "healthy/naïve" (no disease/immunization) or "immune" (sick/vaccinated/immunized) donors. These variable regions are assembled into small antigen binding units such as scFvs, and are fused to the phage G3P coat protein for phage surface expression, thereby generating a phage display library in which each phage expresses a unique scFv-G3P fusion [3, 4]. These libraries are used for biopanning against a specific antigen [5]. Biopanning consists of four basic steps: scFv-phage binding to antigen, washing to reduce unspecific phage binding, elution of bound scFv-phages, and infection of bacteria with eluted bound phages to generate enriched sub-libraries [6]. This cycle is repeated for 2-4 rounds until specific binders are enriched and identified [2, 6-9].

Supplementary methods

mVCAM-1 DNA sequence for mVCAM-1-eGFP vector design

The DNA sequence encoding the open reading frame of mouse VCAM-1 (Uniprot ID P29533) was codon optimized for expression in *Cricetulus griseus* (CHO cells). A Kozak sequence, and NheI, BamHI, and EcoRI restriction sites were added to the 5' and 3' ends for cloning purposes, as shown below.

Optimized sequence with NheI and KOZAK at the 5' end and BamHI-stop-EcoRI at the 3' end:
GCTAGCcacc
ATGCCAGTGAAGATGGTGGCAGTGCTAGGTGCTTCCACCGTCCTTTGGATTCTGTTCGCC
GTTTCCCAGGCCTTCAAGATCGAGATCAGCCCTGAGTACAAGACCATAGCCCAGATCGGC
GATTCCATGGCCCTGACCTGCTCTACAACCGGCTGTGAATCTCCACTGTTTTCCTGGCGG
ACACAGATCGACTCCCCACTGAACGCCAAGGTGAGAACCGAGGGCTCTAAGTCCGTGCTG
ACCATGGAACCTGTGTCCTTCGAGAACGAACACTCTTACCTGTGCACCGCTACCTGCGGC
TCCGGCAAACTGGAGCGCTCCATCCACGTGGACATCTACTCATTTCCCAAGGACCCTGAG
ATCCAGTTCTCTGGCCCTCTGGAAGTGGGGAAGCCTGTGACAGTGAAGTGCCTGGCTCCT
GACATCTACCCTGTGTACAGACTGGAAATCGACCTGTTCAAGGGCGATCAGCTGATGAAC
AGACAAGAGTTCTCCTCTGAAGAGATGACCAAGTCTCTGGAGACAAAGTCTTTGGAGGTC
ACCTTCACCCCCGTGATCGAAGACATCGGAAAGGCTCTGGTGTGCAGAGCCAAACTGCAC
ATCGACCAGATCGATTCTACACTCAAAGAGAGAGAGACAGTGAAGGAGCTCCAAGTGTAC
ATCTCCCCTAGAAACACCACTATCTCTGTGCATCCTTCCACCAGACTGCAAGAGGGCGGC
GCCGTGACCATGACCTGCTCCTCTGAGGGCCTGCCTGCCCCTGAGATCTTCTGGGGACGG
AAGCTGGACAACGAGGTGCTGCAGCTGCTGTCTGGAAATGCCACCCTGACACTGATCGCC
ATGCGGATGGAAGATTCCGGCGTGTACGTGTGCGAGGGAGTGAACCTGATCGGCCGGGAC
AAGGCCGAGGTGGAACTGGTCGTGCAGGAAAAGCCCTTCATCGTGGATATTTCCCCTGGC

AGCCAGGTGGCTGCTCAGGTGGGAGATTCCGTGGTGTTGACATGTGCTGCCATCGGCTGC
GACTCCCCCTCTTTCTCCTGGCGGACCCAGACCGACTCGCCTCTGAACGGCGTAGTGAGA
AACGAGGGCGCTAAGTCTACCCTCGTGCTGTCTTCTGTCGGCTTCGAGGACGAGCATTCT
TACCTGTGTGCTGTGACCTGCCTGCAGAGAACCCTGGAGAAGCGGACCCAGGTGGAAGTG
TACAGCTTCCCTGAGGACCCTGTAATCAAGATGTCCGGACCTCTGGTCCACGGCAGACCC
GTGACCGTTAACTGCACCGTGCCCAACGTCTATCCTTTCGACCACCTGGAGATCGAGCTG
CTGAAGGGCGAAACCACACTGATGAAGAAGTACTTCCTGGAAGAAATGGGCATCAAGAGC
CTTGAGACCAAGATCCTGGAAACCACCTTTATCCCTACAATCGAGGATACCGGCAAGTCC
CTGGTGTGTCTGGCCCGGCTGCACTCCGGCGAGATGGAATCCGAGCCTAAGCAGCGGCAG
TCCGTGCAGCCTCTGTACGTGAACGTGGCCCCTAAGGAAACCACCATCTGGGTGTCCCCT
AGTCCCATCCTGGAGGAAGGCTCCCCAGTGAATCTGACCTGTTCTTCCGATGGCATCCCA
GCGCCTAAGATCCTGTGGTCCAGACAGCTGAACAACGGCGAGCTGCAGCCCCTGAGCGAG
AATACCACCCTGACCTTCATGAGCACCAAGAGAGACGACTCTGGAATCTATGTGTGCGAA
GGCATCAACGAGGCCGGCATCAGCCGGAAGTCCGTGGAACTGATCATCCAAGTGTCTCCT
AAAGACATCCAGCTGACCGTGTTCCCCTCCAAGTCCGTGAAAGAGGGCGACACCGTGATC
ATCTCCTGCACCTGTGGCAACGTGCCTGAGACCTGGATCATCCTGAAGAAGAAAGCTAAG
ACAGGCGACATGGTCCTGAAGTCCGTGGACGGCTCCTACACCATCAGACAGGCCCAGCTG
CAGGACGCTGGCATCTACGAGTGCGAGTCTAAGACCGAGGTGGGCTCTCAGCTCCGCTCC
CTGACATTGGACGTGAAGGGGAAAGAGCACAACAAGGACTACTTCTCTCCTGAGCTGCTG
GCTCTGTACTGCGCCAGCTCCCTGGTGATCCCTGCCATCGGCATGATCGTGTACTTTGCC
AGAAAGGCCAACATGAAGGGCTCCTACTCTCTGGTGGAAGCTCAGAAATCTAAAGT
GGATCCatgagaattc

Generating the scFv-LPETG versions via site-directed mutagenesis

To generate a pET28b_LPETG vector, the following sequence ttaaCCATGGGATATCAAGCTT GCGGCCGC**CTGCCAGAAACCGGT**CTCGAGttaa was added to pET28b (equivalent to ttaa-NcoI-EcoRV-*HindIII*-NotI-**LPETG**-XhoI-ttaa). To do this, two oligomers covering this entire sequence complementary to each other (Sigma Aldrich) were resuspended to a final concentration of 100 mM and annealed together in a thermocycler. Annealing was achieved by heating the sample to 95 °C for 2 minutes and slowly cooling down to 25°C, over a span of 45 minutes. The annealed oligomers were then digested with the restriction enzymes NcoI and XhoI (New England BioLabs® Inc.). An empty pET28b vector was digested simultaneously with the same enzymes, dephophorylated with alkaline phosphatase, and purified using the Qiagen Qiaquick Gel Extraction Kit. Following the digestion of the annealed oligos, the enzymes were heat inactivated at 80 °C for 20 minutes before ligating the annealed oligo with the purified, linearized pET28b vector. The ligation was incubated at 16 ˚C overnight followed by heat inactivation of the enzymes at 65 °C for 10 minutes and then the reaction was held at 4 °C in the Veriti™ 96-Well Thermal Cycler (Applied Biosystems™, 4375786). The ligation was transformed into competent *E. coli* DH5a cells following standard protocols to generate pET28b-LPETG*. The next day the colonies were tested by colony PCR and verified by sequencing, as described in section 3.6. A frameshift was inadvertently incorporated in the sequence during the design. To correct this frameshift, site-directed mutagenesis was performed using the following primers, LPETG codon corrected FWD

(ACTGCCAGAAACCGGTCTCG) and LPETG codon corrected REV (GCGGCCGCAAGCTTGATATCC) (**Supplementary Table S3**). The binding of the FWD primer introduces an overhang of 1 base pair which will be amplified with the pET28b-LPETG* plasmid. The Q5® High-Fidelity DNA Polymerase was used to amplify the vector following manufacturer's recommendations and considering the primers annealing temperature. The PCR product was purified using the QIAquick® PCR Purification Kit (Qiagen) and the linearized DNA was phosphorylated by T4 PNK (New England BioLabs® Inc.) using 100 ng of the purified linear DNA in a reaction mixture containing 5 mL of T4 PNK Reaction Buffer (10X), 5 mL of ATP (10 mM), 1 mL of T4 PNK and nuclease free water to a final volume of 50 mL. The reaction was incubated for 30 minutes at 37 °C and the enzymes were heat inactivated at 65 °C for 20 minutes. The phosphorylated DNA was then ligated using T4 ligase and the ligation transformed into competent *E. coli* DH5a cells to generate plasmid pET28b-LPETG (LZCBI53). Next, the DNA encoding the selected scFvs was subcloned from the phagemid vectors into pET28b(+)-LPETG (LZCBI53) vector through NcoI and NotI double restriction digestion and ligation (Supplementary Table S2). All vectors were sequenced.

mVCAM-1 mutagenesis strategy to generate Ig-like domain mutants

The deletion of mVCAM-1 Ig-like domain(s) starts and ends in the middle of the inter-domain sequence immediately before or immediately after the domain(s) deleted. All mutagenesis procedures were performed using Q5 High-Fidelity DNA Polymerase (NEB, M0491) and primers described in **Supplementary Table S3**. To make these constructs, an N-terminal FLAG tag was first introduced after the signal sequence into LZCBI18 to generate pEGFP-N1_mVCAM-1(1-24)-FLAG-mVCAM1(25-793) (LZCBI120) using primers mVCAM-1 FLAG Fwd and mVCAM-1-FLAG Rev (**Supplementary Table S3**). All Ig-like deletions were made on the LZCBI120 backbone, and 9 different constructs were made: ΔIg-like-1 (primers mVCAM1-d1 Fwd and mVCAM1-d1 Rev), ΔIg-like-1-2 (primers mVCAM1-d2 Fwd and mVCAM1-d1 Rev), ΔIg-like-1-3 (primers mVCAM1-d3 Fwd and mVCAM1-d1 Rev), ΔIg-like-4-7 (primers mVCAM1-d7 Fwd and mVCAM1-d4 Rev), ΔIg-like-5-7 (primers mVCAM1-d7 Fwd and mVCAM1-d5 Rev), ΔIg-like-6-7 (primers mVCAM1-d7 Fwd and mVCAM1-d6 Rev), ΔIg-like-7 (primers mVCAM1-d7 Fwd and mVCAM1-d7 Rev), ΔIg-like-3 (primers mVCAM1-d3 Fwd and mVCAM1-d3 Rev), and ΔIg-like-5 (primers mVCAM1-d5 Fwd and mVCAM1-d5 Rev) (**Supplementary Table S3**). PCR amplified DNA fragments were cleaned with Nucleospin Gel and PCR clean-up mini kit (Macherey-Nagel, 740609), phosphorylated with T4 polynucleotide kinase (NEB, M0201), ligated with T4 Ligase (NEB, M0202), and transformed into chemical competent *Escherichia coli* DH5alpha strains or ST0213 Stellar competent cells (Takara, 636766).

Supplementary Figures

Expression of mVCAM-1_GFP

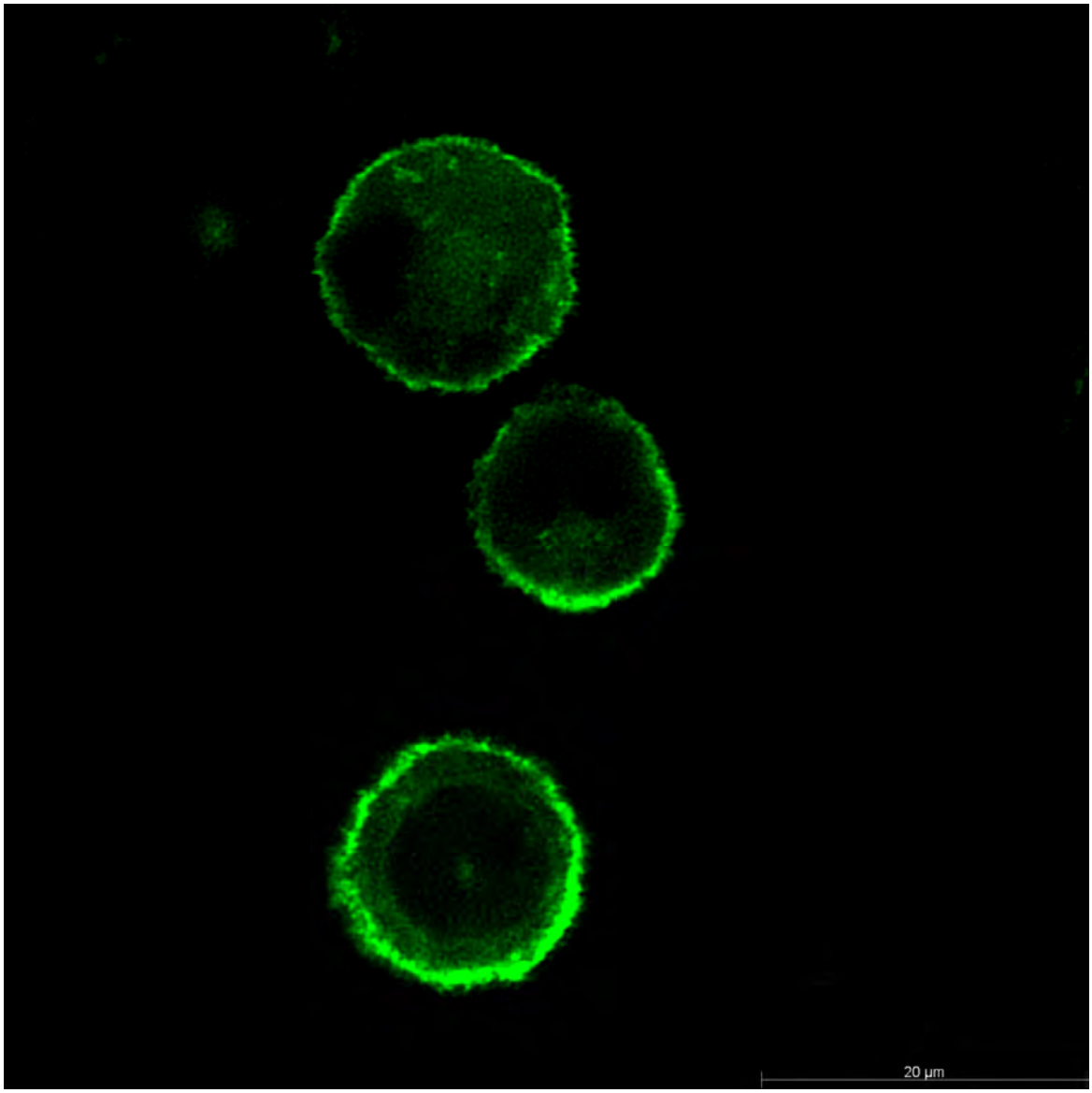

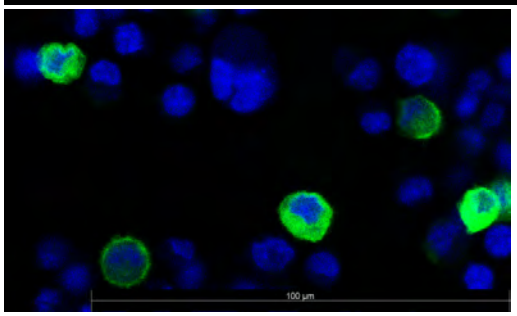

Figure S1. **mVCAM-1-eGFP localizes to the cell periphery in mammalian cells.** Confocal microscopy of CHO XL99 cells transfected with pEGFPN-1_mVCAM-1 showed that mVCAM-1-eGFP is expressed and localized at the cell periphery. The DAPI+GFP overlay image also shows non-expressing cells, demonstrating that the green fluorescence observed is indeed mVCAM-1-eGFP, and not autofluorescence of the cells. Images courtesy of Zhao Wang, Rowan Lab, The University of Queensland.

Biopanning –flow cytometry of phage pools

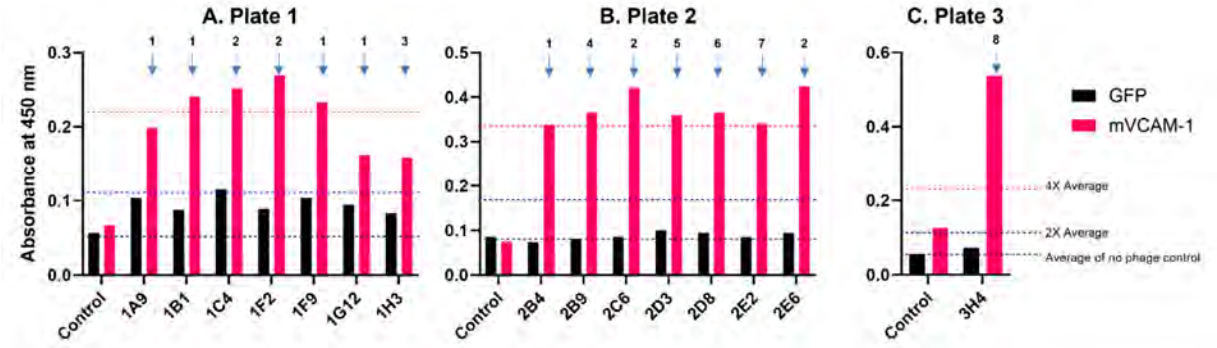

Supplementary Figure S2. Monoclonal whole cell ELISA of round 2 phage pool showed 15 positive clones. Three 96-well plates with individual clones from round 2 phage pool were screened, and the 15 positive clones identified from Plate 1 (**A**), Plate 2 (**B**), and Plate 3 (**C**) are shown. The black line in the graphs indicates the average of the no phage controls in each plate, and the blue and red lines indicate 2-times and 4-times the value of this average, respectively. There are two negative controls in this experiment. First, cells expressing eGFP or mVCAM-1-eGFP incubated only with primary and secondary antibodies but with no phages. The absorbance value of these no-phage controls determined the value of the black line: average of no-phage controls (black line). Second, cells expressing eGFP incubated with phages. When testing the specific isolated phage clones, our criteria to select a positive clone required that the absorbance of a particular phage clone on the eGFP negative control would not exceed 2-times the value of the no phage controls (blue line), and that the corresponding absorbance on the mVCAM-1-eGFP expressing cells was equal or above 4-times the value of the no phage controls (red line). The reason we allowed higher absorbance on the eGFP-only cells above the no phage control is to account for the possibility that inefficient washes or phage stickiness eliminate perfectly good candidates as false negatives. The 4-times above the average requirement to determine a true positive increased the stringency for selection, thereby reducing the chances of selecting false positives. Many of the recovered clones shared the same DNA sequence. All unique positive sequences are listed with a number on the graph, with positive clones with identical sequences sharing the same number.

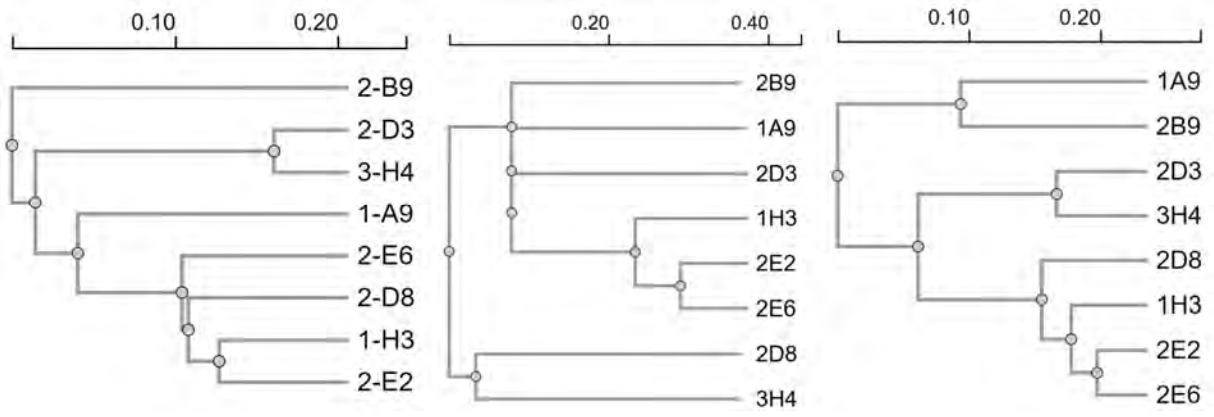

Supplementary Figure S3. Phylogenetic tree of the 8 unique scFv sequences identified. A phylogenetic tree was generated using the entire amino acid sequence of the 8 unique scFvs identified, using Clustal Omega, to facilitate comparing similarities among sequences. The alignment on the left shows the phylogenetic tree for the entire scFv sequences, which reflects differences and similarities in all CDRs and frameworks, while the one on the middle is only for the CDR3 of heavy chains, and the one on the right is only for the entire light chains. As observed on the left and on the right, clones 2D3 and 3H4 are very similar overall and, coincidentally, they also bind the same Ig-like domain in mVCAM-1. As observed on the right, 1A9 and 2B9 are clearly separated from the other antibodies since these two contain kappa light chains while the others contain lambda light chains. Also as observed, on the right, clones 2E2 and 2E6 cluster closely together as they share an almost identical light chain (even though they bind two different Ig-like domains, suggesting a higher role for the heavy chain in determining the epitope).

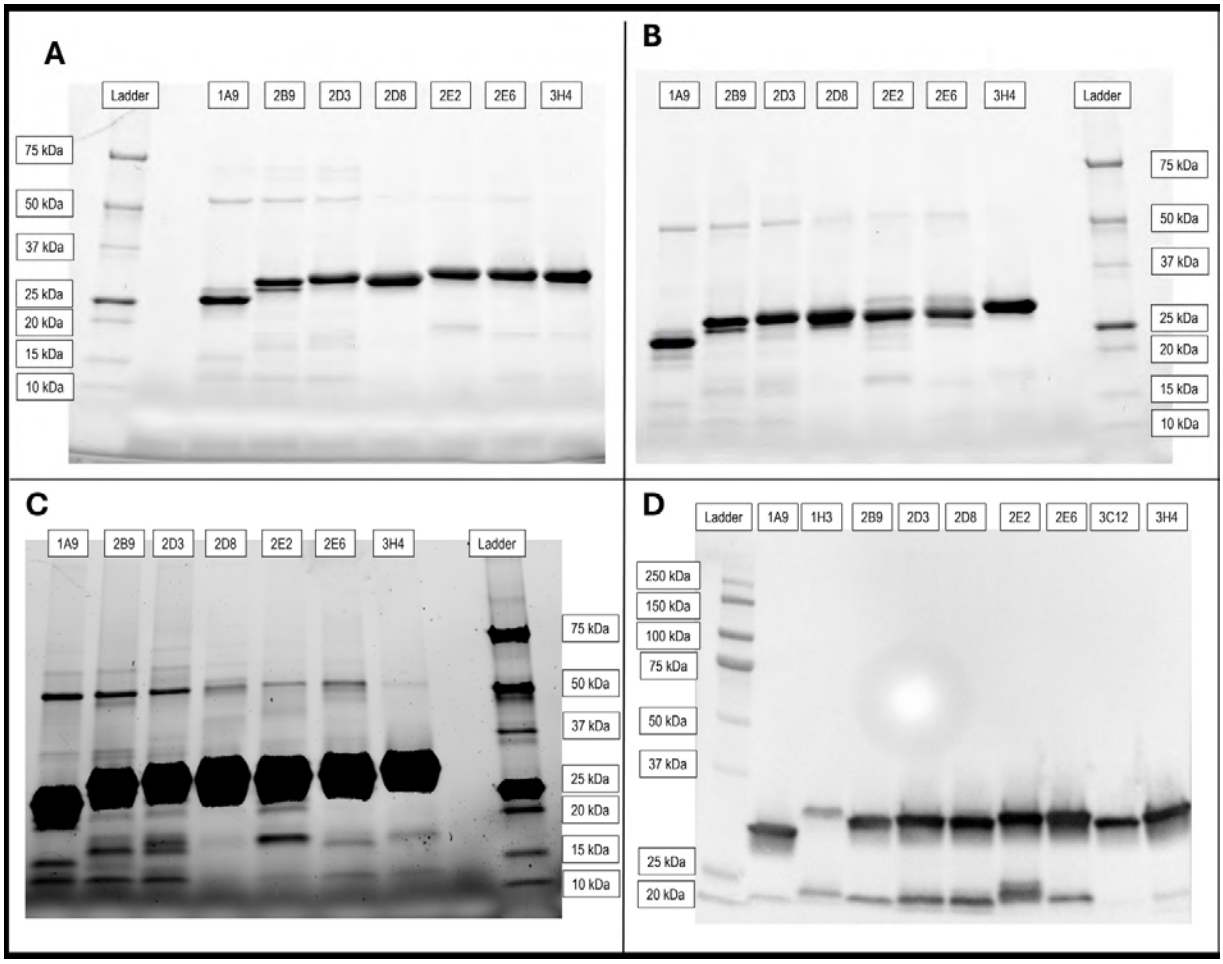

Supplementary Figure S4. **SDS-PAGE of purified scFv-LPETG clones, and western blot of cell extracts pre-purification.** Reducing **(A)** or non-reducing **(B,C)** SDS-PAGE of purified scFv-LPETGs. Panel (**C***)* is an overexposed version of the gel in **(B)**. The gels were loaded with 5 µg of purified scFv-LPETG of clones 1A9, 2B9, 2D3, 2D8, 2E2, 2E6, and 3H4. **D)** Western blot of whole cell extracts from SHuffle *E. coli* strains expressing the different scFv-LPETGs prior to purification. The blot was prepared as described in the methods in the main text. The anti-His-HRP (Miltenyi Biotec Cat# 130-092-785, RRID:AB_1103231) antibody used was at a 1:5,000 dilution.

We note that this figure contains the clones 1H3 (**D**), 2B9 (**A-D**), and 3C12 (**D**). As described in the main text, clones 1H3 and 2B9 were not further pursued due to potential sequence liabilities when expressed in eukaryotic cells, as explained in the results section. Clones 2B9 and 3C12 bound to mVCAM-1 expressing cells with high specificity, while clone 1H3 showed extensive background binding (data not shown). Clone 3C12 has not been discussed in this manuscript.

The antibodies were purified with varied levels of purity, and additional proteins can be seen co-purifying with the antibodies with different relative abundances. Mass spectrometry analysis of one of the purified scFv samples (clone 2D8) showed that the 3 most abundant co-purified proteins had MW in the range of 55-70 kDa (see **Supplementary Table S5**). Bands with similar MW to

these three proteins were generally observed in all purified scFvs and scFvs-LPETG clones (**Supplementary Figure S4** and data not shown). We observed similar behaviour of the scFv-LPETG tagged antibodies compared to the scFv antibodies in the SDS-PAGE from purified samples, western blot from cell extracts pre-purification, and by flow cytometry (data not shown) indicating that, as expected, the tag is unlikely to have an impact on antibody expression and function.

We note that in the western blot (**Supplementary Figure S4D**) there is an ~15 kDa or lower MW band reactive with anti-HIS antibody observed in all the cell extracts, with different intensity levels. These bands could be partially cleaved antibodies that still contain the C-terminus. However, these lower MW fragments are either not observed in the purified material or present at considerably lower relative abundances (compare D with B,C), possibly because the fragments were lost during the dialysis step. Therefore, these lower MW fragments (containing the light variable chain) are unlikely to have had any impact on the subsequent functional analysis performed on these antibodies.

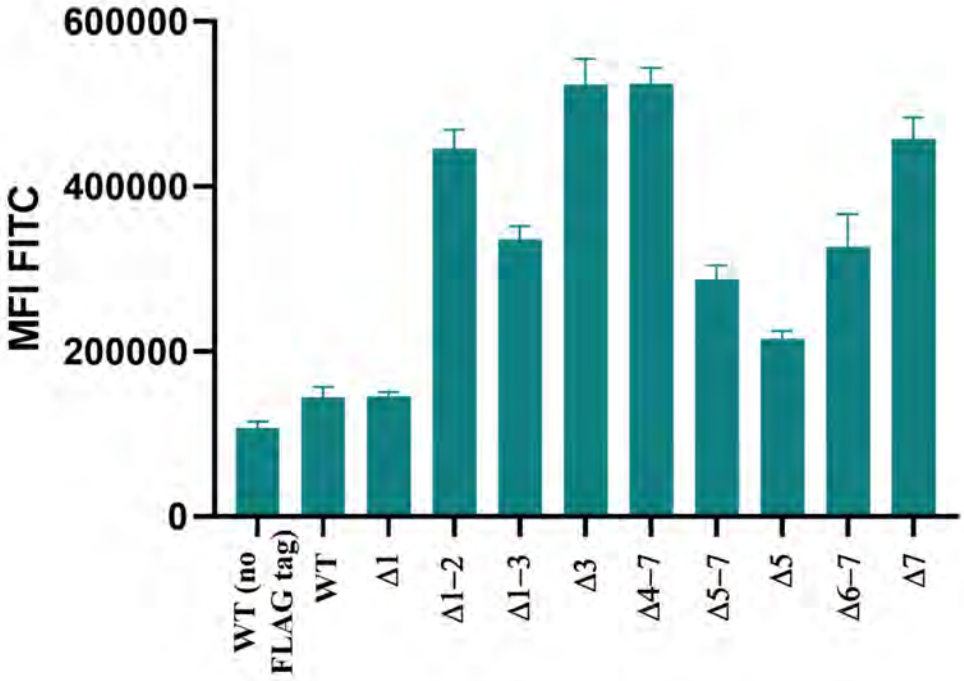

Supplementary Figure S5. **Flow cytometry data comparing GFP expression for all Ig-like domain mutants.** ExpiCHO cells transiently transfected with mVCAM-1-eGFP WT (with or without N-terminal FLAG) or FLAG-tagged mVCAM-1-eGFP Ig-like deletion constructs were used for flow cytometry as described in the methods. Overall expression efficiency of the constructs was determined using GFP expression (FITC signal). Results represent the average MFI (FITC-H) +/- SE from one experiment with 21 replicates for each vector. The data shows that addition of the FLAG tag or deletion of Ig-like domain 1 only marginally increased the overall GFP expression in transfected cells. However, all other constructs showed a larger increase in GFP signal that did not always correlate with anti-FLAG antibody binding (a marker for cell surface expression, **Figure 4**, **Supplementary Figure S6**) and could indicate intracellular accumulation of GFP (potentially due to folding defects). Importantly, the Δ5-7 Ig-like mutant construct (which showed poor binding to all antibodies tested, **Figure 4, Supplementary Figure S6**) showed higher overall GFP expression than the controls WT mVCAM-1 with or without N-terminal FLAG tag), demonstrating that lack of antibody binding to this construct by flow cytometry was not due to lower overall construct expression.

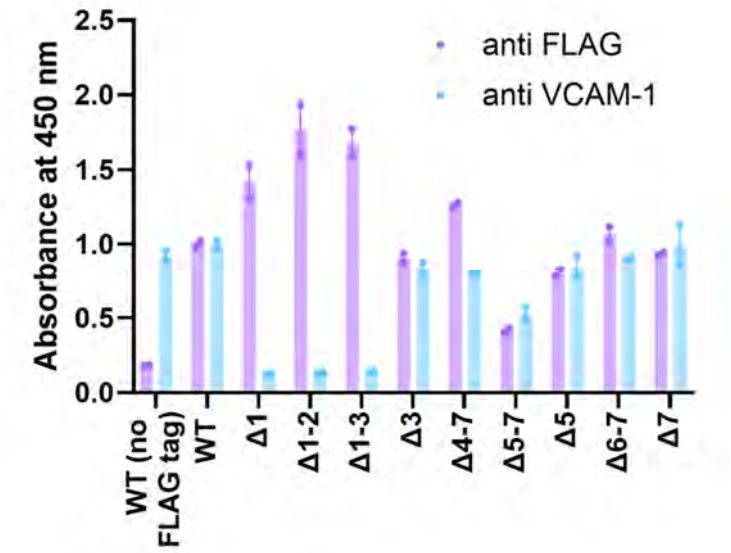

Supplementary Figure S6. **Whole cell ELISA comparing cell surface expression for mVCAM-1-eGFP constructs.** ExpiCHO cells transiently transfected with mVCAM-1-eGFP WT (with or without N-terminal FLAG) or FLAG-tagged mVCAM-1-eGFP Ig-like deletion constructs were used for whole cell ELISA. In this experiment, $5x10^5$ cells/well were stained with either 1:400 rabbit anti-FLAG (Cell Signaling Technology Cat# 2368, RRID:AB_2217020) or 1:400 rat anti-VCAM-1 CBL1300 (Millipore Cat# CBL1300, RRID:AB_2214062) primary antibodies, followed by 1:1,000 anti-rabbit IgG-HRP (Cell Signaling Technology Cat# 7074, RRID:AB_2099233) or 1:1,000 anti-rat IgG-HRP (Cell Signaling Technology Cat# 7077, RRID:AB_10694715) secondary antibodies. Graphs show the average-Max-Min of the Absorbance at 450 nm from one experiment with 2 replicates for each vector. All results are normalized to the values of the mVCAM-1-eGFP-FLAG tagged WT vector. The results of this experiment are in complete agreement with the results from the flow cytometry experiment (**Figure 4**), and support that: 1) addition of the FLAG tag did not lead to a decrease in cell surface expression of the mutant mVCAM-1 versions; 2) CBL1300 binds mVCAM-1 Ig-like domain 1 (and **Supplementary Table S1**); and 3) cell surface expression of the Δ5-7 Ig-like mutant construct is less efficient compared to the other constructs (the differences between the flow cytometry data in **Figure 4** and the ELISA data in this figure are likely due to differences in the sensitivity of the assays in these specific experimental conditions, and support that this construct is indeed at least partially expressed on the cell surface (see discussion)).

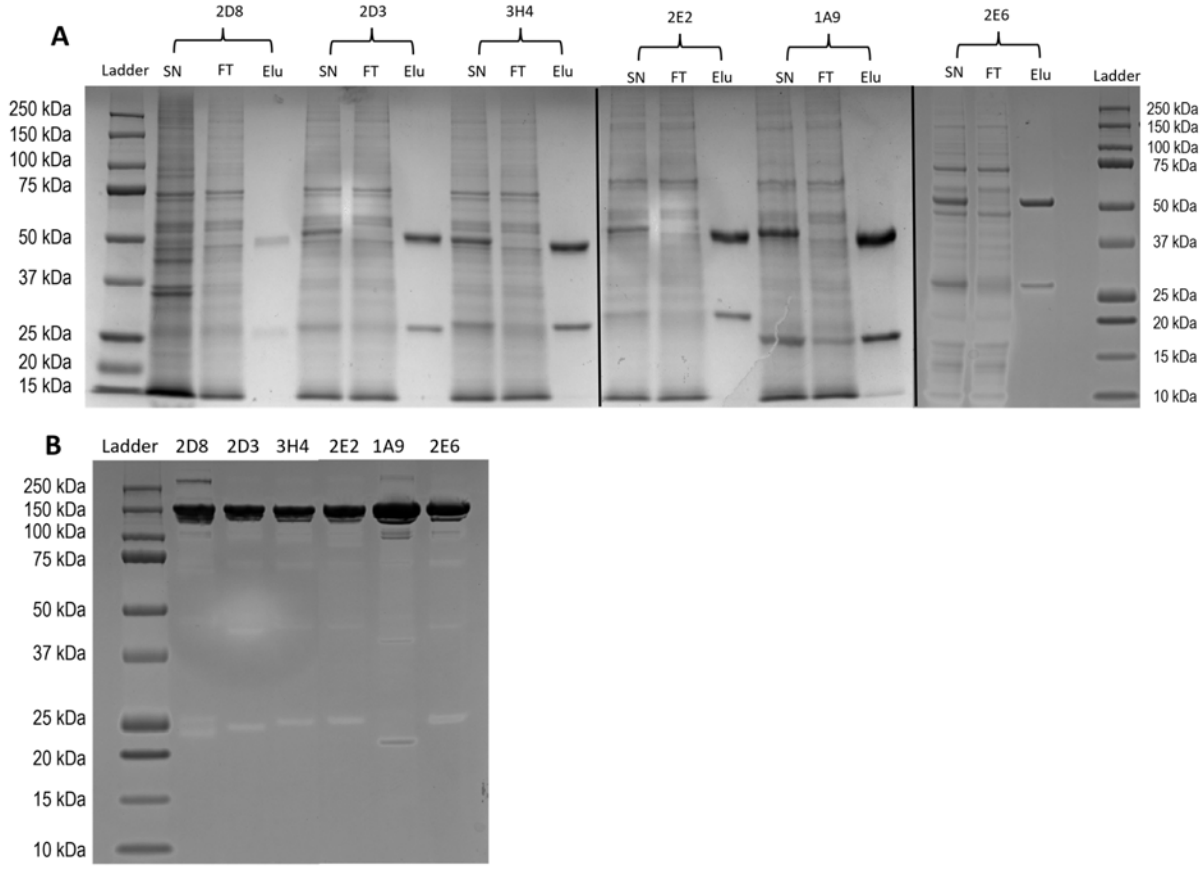

Supplementary Figure S7. Reducing and non-reducing SDS-PAGEs of full-length reformatted IgG2a monoclonal anti-mVCAM-1 antibodies. A) Reducing SDS-PAGE of the supernatant (SN), Flow-through (FT), and 5 µg of purified mAb (Elu) for clones 1A9, 2D3, 2D8, 2E2, 2E6, and 3H4. **B)** Non-reducing SDS-PAGE showing 5 µg of purified mAb for clones 1A9, 2D3, 2D8, 2E2, 2E6, and 3H4.

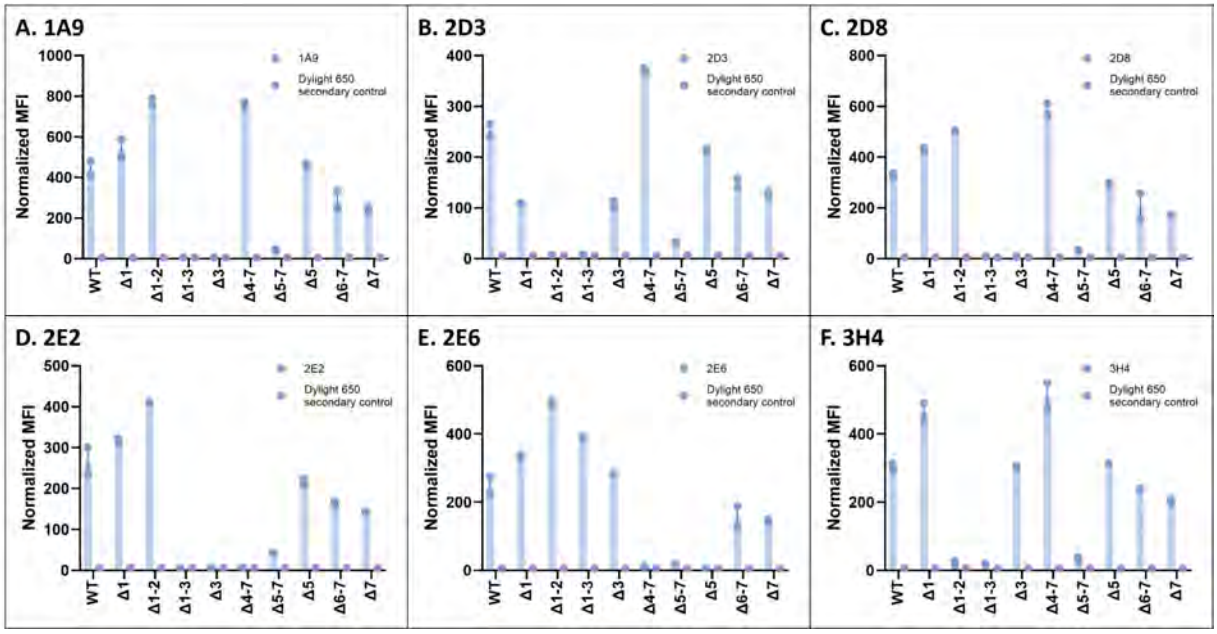

Supplementary Figure S8: Ig-like domain mapping of the isolated antibodies. Flow cytometry analysis of the binding of our new six full-length IgG2a reformatted antibodies to cells transiently transfected with mVCAM-1-eGFP WT (with or without N-terminal FLAG) or FLAG-tagged Ig-like deletion constructs. The secondary antibody only treatment is shown as negative control (Dylight 650). Displayed is the average normalized MFI-Max-Min (mVCAM-1-eGFP-positive, antibody positive cells normalized to MFI of the mVCAM-1-eGFP-negative, antibody negative cells) from one experiment with 2 replicates.

Supplementary Tables

Supplementary Table S1. Non-exhaustive list of antibodies developed against VCAM-1, their targeted domain (if known), and the associated function. This table is only a snapshot of some of the reagents that have been developed to study VCAM-1 and it is not comprehensive. We apologise in advance as there are many antibodies and/or their functional assays that we have not included below.

Antibody	**Domain targeted**	**Impact of antibody on VCAM-1 function** (domain associated)	**Reference**
4B9	1 (And 4?)[1]	Inhibits adherence of PBL and lymphocytic cell line (not neutrophils) to activated HUVE. May be important for lymphocyte emigration and immune response.	[10-13]
ED11, GH12, and GE4	4, different epitopes	ED11 and GH12 can block VLA-4 dependent binding to VCAM-1 in certain genetic scenarios (e.g. absence of domain 1), although ED11 significantly blocked binding of Ramos cells to activated endothelial cells (ECs).	[12]
H6	1-2	Blocks adhesion and transmigration between VCAM-1 and inflammatory cells.	[14]
7H	1-2	Blocks adhesion and transmigration. In ApoE$^{-/-}$ mice, 7H reduces the effect of atherosclerosis.	[14]
MVCAM.A[2] 429	1-2	Reduces eosinophil infiltration on skin.	[15, 16] and [2]
M-/K1 and M-/K2[3]	1 and 4	Inhibit binding of VLA-4 expressing cells to VCAM-1. Prevent lymphopoiesis. Prevent binding of lymphoid cells to activated EC. Reduces inflammation. Enhances survival rates of grafts. Blocks cardiomyocyte hypertrophy, myofibroblast activation, and cardiac remodelling (M/K2.7).	[17-21] and [3]
2G7	1-3[4]	Blocks binding of T cells to activated ECs. Blocks adhesion of basophils and eosinophils to activated ECs. Blocks activation of CD4+ T cells.	[22-24] [5]
1E7	1-3[4]	Does not block activation of CD4+ T cells. Different epitope than 2G7.	[22, 24] [5]
1G11, 1E5, 1.4C3, 6D9	?	1G11 and 1E5 block T cell adhesion to ECs, but 14C3 and 6D9 do not. All antibodies react with the circulatory VCAM-1 form, so they are not D4 only binders. IG11 also blocks VCAM-1 mediated survival of neutrophils, and blocks VLA4-mediated release of interleukins by monocytes.	[25-27]
BBIG-V1[6]	1	Blocks VLA4-mediated release of interleukins by monocytes.	[27]
BBIG-V4	3		[28]
19C3	2		[28, 29]
1E10[7]	1	Likely BBIG-V3	[28, 29]
E1/6	1	Blocks binding to VLA4. Prevents melanoma and other tumors adhering to activated ECs. Inhibits binding of lymphoid cells to activated ECs. Epitope of E1/6 is different from 4B9 (see above).	[11, 30-32]
Hu8/4	4-7	Does not inhibit binding of melanoma to activated ECs.	[30]

VCAM-1 D6 Fab	6	Blocks leukocyte transendothelial migration.	[33]
1/9	Likely 1 and/or 4	Blocks eosinophils rolling *in vivo* (likely by blocking domains 1 and/or 4).	[34]
51-10C9	1	Blocks leukocyte adhesion. Enhanced TNF-α–stimulated EC production of IL-8.	[33]
1.G11B1[8]		Decrease in eosinophil tethering to IL-4 stimulated HUVECs particularly at high shear stress. Inhibits cell adhesion between B cells and FLS (fibroblast-like σψνοϖιοχψτεσ).	[35, 36]
HD101	1 and 2	Inhibits cell adhesion. Induces VCAM-1 internalization into the cytoplasm. Anti-inflammatory and anti-asthma effects.	[37]
Antibody against VLA-4			
Natalizumab[9]	*α4β1 integrin blocker*	*Blocks interaction with VCAM-1 domains 1 and 4. Treatment for multiple sclerosis and Chron's disease.*	

[1] Vonderheide and Springer [11] suggest that 4B9 binds to both Ig-like domains 1 and 4, but Osborn et al [38] data shows that it only binds 1 and suggests that it can sterically hinder interaction with domain 4 due to its size/position or possibly by perturbing the conformation/structure of the molecule upon binding.

[2] https://www.bdbiosciences.com/en-us/products/reagents/flow-cytometry-reagents/research-reagents/single-color-antibodies-ruo/fitc-rat-anti-mouse-cd106.553332

[3] https://www.merckmillipore.com/AU/en/product/Anti-VCAM-1-Antibody-clone-M-K,MM_NF-CBL1300?ReferrerURL=https%3A%2F%2Fwww.google.com%2F

[4] But could potentially also recognise other Ig-like domains that were not tested.

[5] From W. Newman, Otsuka America Pharmaceutical.

[6] https://www.rndsystems.com/products/human-vcam-1-cd106-antibody-bbig-v1_bba5

[7] https://www.rndsystems.com/products/human-vcam-1-cd106-fluorescein-conjugated-antibody-bbig-v3-ie10_bba22

[8] https://www.bio-rad-antibodies.com/monoclonal/human-cd106-antibody-1-g11b1-mca907.html?f=purified

[9] https://go.drugbank.com/drugs/DB00108

Supplementary Table S2. Plasmids constructed and used in this study.

Plasmid	Alias
pUCIDT_mVCAM-1	LZCBI 17
pEGFP-N1_mVCAM-1	LZCBI 18
pET28b-1A9	LZCBI 41
pET28b-2D3	LZCBI 45
pET28b-2D8	LZCBI 46
pET28b-2E2	LZCBI 47
pET28b-2E6	LZCBI 48
pET28b-3H4	LZCBI 50
pET28b-LPETG	LZCBI 53
pET28b-2D3-LPETG	LZCBI 54
pET28b-2D8-LPETG	LZCBI 55
pET28b-2E6-LPETG	LZCBI 56
pET28b-3C12-LPETG	LZCBI 57
pET28b-3H4-LPETG	LZCBI 58
pET28b-1A9-LPETG	LZCBI 87
pET28b-1H3-LPETG	LZCBI 88
pET28b-2B9-LPETG	LZCBI 89
pET28b-2E2-LPETG	LZCBI 90
NBF320 JW8_ExpMG2a_2D3_Heavy chain	LZCBI 106
NBF320 JW8_ExpMG2a_2E2_Heavy chain	LZCBI 108
NBF320 JW8_ExpMG2a_2E6_Heavy chain	LZCBI 109
NBF320 JW8_ExpMG2a_1A9_Heavy chain	LZCBI 110
NBF320 JW8_ExpMG2a_3H4_Heavy chain	LZCBI 111
NBF320 JW8_ExpMG2a_2D8_Heavy chain	LZCBI 112
NBF372 JW8_ExpMG2a_2D3_Light chain	LZCBI 113
NBF372 JW8_ExpMG2a_2E2_Light chain	LZCBI 115
NBF372 JW8_ExpMG2a_2E6_Light chain	LZCBI 116
NBF321 JW8_ExpMG2a_1A9_Light chain	LZCBI 117
NBF372 JW8_ExpMG2a_2D8_Light chain	LZCBI 118
NBF372 JW8_ExpMG2a_3H4_Light chain	LZCBI 119
pEGFP-N1_mVCAM-1(1-24)-FLAG-mVCAM1(25-793)	LZCBI 120
pEGFP-N1_mVCAM-1(1-24)-FLAG-mVCAM1(25-793)_ΔIgG_like_1	LZCBI 121

pEGFP-N1_mVCAM-1(1-24)-FLAG-mVCAM1(25-793)_ΔIgG_like_1-2	LZCBI 122
pEGFP-N1_mVCAM-1(1-24)-FLAG-mVCAM1(25-793)_ΔIgG_like_1-3	LZCBI 123
pEGFP-N1_mVCAM-1(1-24)-FLAG-mVCAM1(25-793)_ΔIgG_like_4-7	LZCBI 124
pEGFP-N1_mVCAM-1(1-24)-FLAG-mVCAM1(25-793)_ΔIgG_like_5-7	LZCBI 125
pEGFP-N1_mVCAM-1(1-24)-FLAG-mVCAM1(25-793)_ΔIgG_like_6-7	LZCBI 126
pEGFP-N1_mVCAM-1(1-24)-FLAG-mVCAM1(25-793)_ΔIgG_like_7	LZCBI 127
pEGFP-N1_mVCAM-1(1-24)-FLAG-mVCAM1(25-793)_ΔIgG_like_3	LZCBI 129
pEGFP-N1_mVCAM-1(1-24)-FLAG-mVCAM1(25-793)_ΔIgG_like_5	LZCBI 130

Supplementary Table S3. Primers used in this study.

Name	Sequence
mVCAM1-FLAG Fwd	ACGACGACGACAAGTTCAAGATCGAGATCAGC
mVCAM1-FLAG Rev	CCTTGTAGTCGGCCTGGGAAACGGCGA
mVCAM1-d7 Fwd	TTGGACGTGAAGGGGAAAGAGC
mVCAM1-d7 Rev	AGACACTTGGATGATCAGTTCC
mVCAM1-d6 Rev	GGCCACGTTCACGTACAGAGG
mVCAM1-d5 Rev	AGGGTCCTCAGGGAAGCTGTACAC
mVCAM1-d4 Rev	CTTTTCCTGCACGACCAGTTCCAC
mVCAM1-d1 Fwd	ATCTACTCATTTCCCAAGGACCCTG
mVCAM1-d1 Rev	CTTGTCGTCGTCGTCCTTGTAGTC
mVCAM1-d2 Fwd	ACAGTGAAGGAGCTCCAAGTG
mVCAM1-d3 Fwd	GAAAAGCCCTTCATCGTGG
mVCAM1-d3 Rev	GGAGATGTACACTTGGAGCTC
mVCAM1-d5 Fwd	GTGAACGTGGCCCCTAAGG
LPETG codon corrected Fwd	ACTGCCAGAAACCGGTCTCG
LPETG codon corrected Rev	GCGGCCGCAAGCTTGATATCC

Supplementary Table S4. Protein parameters for purified scFv-LPETG antibodies.

Sample	Molecular weight (Da)	Extinction Coefficient	Theoretical pI
1A9	28038.20	52620	8.3
2D3	27980.87	57090	6.99
2D8	27337.19	46090	7.07
2E2	27183.86	43110	8.30
2E6	27976.79	54110	6.14
3H4	27209.86	54110	6.58

Supplementary Table S5. Summary of co-eluting proteins identified by Mass Spectrometry proteomics with Proteome Discoverer Software. The three proteins with the highest number of peptide spectrum matches (PSMs) are shown.

Accession #	Description	Coverage [%]	# Peptides	# PSMs	# Unique Peptides	# AAs	MW [kDa]	calc. pI	# Peptides (by Search Engine): Sequest HT
P35340	Alkyl hydroperoxide reductase subunit F OS=Escherichia coli (strain K12) OX=83333 GN=ahpF PE=1 SV=2	53	32	355	32	521	56.1	5.68	32
P0A6Y8	Chaperone protein DnaK OS=Escherichia coli (strain K12) OX=83333 GN=dnaK PE=1 SV=2	63	35	150	35	638	69.1	4.97	35
P0A6F5	60 kDa chaperonin OS=Escherichia coli (strain K12) OX=83333 GN=groL PE=1 SV=2	57	28	129	28	548	57.3	4.94	28

We performed mass spectrometry proteomic analysis on one of the purified scFv samples to better understand the composition of the co-eluting proteins in the samples. The results showed three overly represented proteins (as determined by the number of peptide spectrum matches (PSMs) and % of coverage), shown in above. The number of PSMs identified positively correlates with the abundance of their associated protein in the sample. All three identified proteins have MW in the range of 55-70 kDa, which is where the strongest bands that co-elute essentially with all the purified scFvs and scFv-LPETGs appear (**Supplementary Figure S4A-C** and data not shown). Two of these three main proteins were chaperones, Chaperone protein DnaK and 60 kDa chaperonin, which help in protein folding. The third protein was an enzyme, Alkyl hydroperoxide reductase, that prevents DNA damage by alkyl hydroperoxides.

References

1. Sioud, M., *Phage Display Libraries: From Binders to Targeted Drug Delivery and Human Therapeutics.* Mol Biotechnol, 2019. **61**(4): p. 286-303.
2. Bazan, J., I. Calkosinski, and A. Gamian, *Phage display--a powerful technique for immunotherapy: 1. Introduction and potential of therapeutic applications.* Hum Vaccin Immunother, 2012. **8**(12): p. 1817-28.
3. Zhao, A., et al., *Phage antibody display libraries: a powerful antibody discovery platform for immunotherapy.* Crit Rev Biotechnol, 2016. **36**(2): p. 276-89.
4. Bashir, S. and J. Paeshuyse, *Construction of Antibody Phage Libraries and Their Application in Veterinary Immunovirology.* Antibodies (Basel), 2020. **9**(2): p. 21.

5. Lim, C.C., P.C.Y. Woo, and T.S. Lim, *Development of a Phage Display Panning Strategy Utilizing Crude Antigens: Isolation of MERS-CoV Nucleoprotein human antibodies.* Sci Rep, 2019. **9**(1): p. 6088.
6. Ma, H. and R. O'Kennedy, *Recombinant antibody fragment production.* Methods, 2017. **116**: p. 23-33.
7. Alfaleh, M.A., et al., *Strategies for Selecting Membrane Protein-Specific Antibodies using Phage Display with Cell-Based Panning.* Antibodies (Basel), 2017. **6**(3): p. 10.
8. Alfaleh, M.A., et al., *Canine CD117-Specific Antibodies with Diverse Binding Properties Isolated from a Phage Display Library Using Cell-Based Biopanning.* Antibodies (Basel), 2019. **8**(1): p. 15.
9. Jones, M.L., et al., *Targeting membrane proteins for antibody discovery using phage display.* Sci Rep, 2016. **6**: p. 26240.
10. Carlos, T.M., et al., *Vascular cell adhesion molecule-1 mediates lymphocyte adherence to cytokine-activated cultured human endothelial cells.* Blood, 1990. **76**(5): p. 965-70.
11. Vonderheide, R.H. and T.A. Springer, *Lymphocyte adhesion through very late antigen 4: evidence for a novel binding site in the alternatively spliced domain of vascular cell adhesion molecule 1 and an additional alpha 4 integrin counter-receptor on stimulated endothelium.* J Exp Med, 1992. **175**(6): p. 1433-42.
12. Osborn, L., C. Vassallo, and C.D. Benjamin, *Activated endothelium binds lymphocytes through a novel binding site in the alternately spliced domain of vascular cell adhesion molecule-1.* J Exp Med, 1992. **176**(1): p. 99-107.
13. Pepinsky, B., et al., *Structure/function studies on vascular cell adhesion molecule-1.* J Biol Chem, 1992. **267**(25): p. 17820-6.
14. Park, J.G., et al., *Evaluation of VCAM-1 antibodies as therapeutic agent for atherosclerosis in apolipoprotein E-deficient mice.* Atherosclerosis, 2013. **226**(2): p. 356-63.
15. Hakugawa, J., et al., *The inhibitory effect of anti-adhesion molecule antibodies on eosinophil infiltration in cutaneous late phase response in Balb/c mice sensitized with ovalbumin (OVA).* J Dermatol, 1997. **24**(2): p. 73-9.
16. Renz, M.E., et al., *Structural requirements for adhesion of soluble recombinant murine vascular cell adhesion molecule-1 to alpha 4 beta 1.* J Cell Biol, 1994. **125**(6): p. 1395-406.
17. Hession, C., et al., *Cloning of murine and rat vascular cell adhesion molecule-1.* Biochem Biophys Res Commun, 1992. **183**(1): p. 163-9.
18. Miyake, K., et al., *A VCAM-like adhesion molecule on murine bone marrow stromal cells mediates binding of lymphocyte precursors in culture.* J Cell Biol, 1991. **114**(3): p. 557-65.
19. Miyake, K., et al., *Evidence for a role of the integrin VLA-4 in lympho-hemopoiesis.* J Exp Med, 1991. **173**(3): p. 599-607.
20. Gorcyznski, R.M., et al., *Manipulation of skin graft rejection in alloimmune mice by anti-VCAM-1:VLA-4 but not anti-ICAM-1:LFA-1 monoclonal antibodies.* Transpl Immunol, 1995. **3**(1): p. 55-61.
21. Qiu, Z.Y., et al., *Blocking VCAM-1 ameliorates hypertensive cardiac remodeling by impeding macrophage infiltration.* Front Pharmacol, 2022. **13**: p. 1058268.

22. Graber, N., et al., *T cells bind to cytokine-activated endothelial cells via a novel, inducible sialoglycoprotein and endothelial leukocyte adhesion molecule-1.* J Immunol, 1990. **145**(3): p. 819-30.
23. Bochner, B.S., et al., *Adhesion of human basophils, eosinophils, and neutrophils to interleukin 1-activated human vascular endothelial cells: contributions of endothelial cell adhesion molecules.* J Exp Med, 1991. **173**(6): p. 1553-7.
24. Damle, N.K. and A. Aruffo, *Vascular cell adhesion molecule 1 induces T-cell antigen receptor-dependent activation of CD4+T lymphocytes.* Proc Natl Acad Sci U S A, 1991. **88**(15): p. 6403-7.
25. Wellicome, S.M., et al., *Detection of a circulating form of vascular cell adhesion molecule-1: raised levels in rheumatoid arthritis and systemic lupus erythematosus.* Clin Exp Immunol, 1993. **92**(3): p. 412-8.
26. Ross, E.A., et al., *Interaction between integrin alpha9beta1 and vascular cell adhesion molecule-1 (VCAM-1) inhibits neutrophil apoptosis.* Blood, 2006. **107**(3): p. 1178-83.
27. Zohlnhofer, D., et al., *Adhesion of monocyte very late antigen-4 to endothelial vascular cell adhesion molecule-1 induces interleukin-1beta-dependent expression of interleukin-6 in endothelial cells.* Arterioscler Thromb Vasc Biol, 2000. **20**(2): p. 353-9.
28. Dudgeon, T.J., et al., *Expression and characterisation of a very-late antigen-4 (alpha 4 beta 1) integrin-binding fragment of vascular cell-adhesion molecule-1.* Eur J Biochem, 1994. **226**(2): p. 517-23.
29. Newham, P., et al., *Alpha4 integrin binding interfaces on VCAM-1 and MAdCAM-1. Integrin binding footprints identify accessory binding sites that play a role in integrin specificity.* J Biol Chem, 1997. **272**(31): p. 19429-40.
30. Taichman, D.B., et al., *Tumor cell surface alpha 4 beta 1 integrin mediates adhesion to vascular endothelium: demonstration of an interaction with the N-terminal domains of INCAM-110/VCAM-1.* Cell Regul, 1991. **2**(5): p. 347-55.
31. Rice, G.E. and M.P. Bevilacqua, *An inducible endothelial cell surface glycoprotein mediates melanoma adhesion.* Science, 1989. **246**(4935): p. 1303-6.
32. Rice, G.E., J.M. Munro, and M.P. Bevilacqua, *Inducible cell adhesion molecule 110 (INCAM-110) is an endothelial receptor for lymphocytes. A CD11/CD18-independent adhesion mechanism.* J Exp Med, 1990. **171**(4): p. 1369-74.
33. Lee, S., et al., *An antibody to the sixth Ig-like domain of VCAM-1 inhibits leukocyte transendothelial migration without affecting adhesion.* J Immunol, 2012. **189**(9): p. 4592-601.
34. Sriramarao, P., et al., *VCAM-1 is more effective than MAdCAM-1 in supporting eosinophil rolling under conditions of shear flow.* Blood, 2000. **95**(2): p. 592-601.
35. Reparon-Schuijt, C.C., et al., *Regulation of synovial B cell survival in rheumatoid arthritis by vascular cell adhesion molecule 1 (CD106) expressed on fibroblast-like synoviocytes.* Arthritis Rheum, 2000. **43**(5): p. 1115-21.
36. Patel, K.D., *Eosinophil tethering to interleukin-4-activated endothelial cells requires both P-selectin and vascular cell adhesion molecule-1.* Blood, 1998. **92**(10): p. 3904-11.
37. Lee, J.H., et al., *A novel human anti-VCAM-1 monoclonal antibody ameliorates airway inflammation and remodelling.* J Cell Mol Med, 2013. **17**(10): p. 1271-81.
38. Hession, C., et al., *Cloning of an alternate form of vascular cell adhesion molecule-1 (VCAM1).* J Biol Chem, 1991. **266**(11): p. 6682-5.